CHARACTERIZATION OF THE GRAPHITE/EPOXY INTERFACE WITH VARIOUS SURFACE TREATMENTS UNDER CYCLIC LOADING

BY

JAMES PAUL RYAN

B.S., United States Air Force Academy, 1995

THESIS

Submitted in partial fulfillment of the requirements
for the degree of Master of Science in Materials Science and Engineering
in the Graduate College of the
University of Illinois at Urbana-Champaign, 1997

Urbana, Illinois

UNIVERSITY OF ILLINOIS AT URBANA-CHAMPAIGN

THE GRADUATE COLLEGE

MAY 1997
(date)

WE HEREBY RECOMMEND THAT THE THESIS BY

JAMES PAUL RYAN

ENTITLED CHARACTERIZATION OF THE GRAPHITE/EPOXY INTERFACE WITH VARIOUS SURFACE TREATMENTS UNDER CYCLIC LOADING

BE ACCEPTED IN PARTIAL FULFILLMENT OF THE REQUIREMENTS FOR THE DEGREE OF MASTER OF SCIENCE

Director of Thesis Research

Head of Department

Committee on Final Examination†

Chairperson

† Required for doctor's degree but not for master's.

O-517

Characterization of the Graphite/Epoxy Interface With Various Surface Treatments Under Cyclic Loading

James P. Ryan
Department of Materials Science and Engineering
University of Illinois at Urbana-Champaign, 1997
Jian-Ku Shang, Advisor

The effects of graphite surface modification on fatigue crack growth resistance of the graphite/epoxy interface were examined using flexural peel specimens. Edge surfaces of pryolitic graphite were treated in an oxygen plasma for various lengths of time and subsequently bonded to a toughened epoxy to form flexural peel specimens. Fatigue crack growth rates were measured for the plasma treated and untreated specimens as a function of strain energy release rate. Fatigue crack growth resistance of plasma treated specimens was notably higher than that of untreated specimens, with the fatigue threshold doubled at an optimal treatment time. X-ray photoelectron spectroscopy, electron microscopy, and surface profilometry studies indicated that both surface chemistry and surface morphology of the graphite were changed by the plasma treatment. High temperature annealing was used to restore the original surface chemistry while retaining the etched surface morphology. Fatigue experiments were then performed on the heat treated specimens to separate the chemical and morphological effects on resistance to crack growth. Chemical modification turned out to be a secondary effect, contributing less than 13% to the overall fatigue crack growth resistance. A micro-mechanical model is proposed which explains the relative effects of surface chemistry and morphology on fatigue crack growth resistance along the graphite/epoxy interface.

Acknowledgments

I would like to take this opportunity to express my sincere gratitude to those individuals who have taken the time to help in this research effort. Most importantly, I would like to express my sincere gratitude to my thesis advisor, Dr. Jian-Ku Shang, professor, Department of Materials Science and Engineering, for his invaluable support, competent guidance, and insightful suggestions throughout my study.

I would also like to thank the members of the Center for Microanalysis of Materials of the Materials Research Laboratory at the University of Illinois. In particular, I owe thanks to Ms. Irena Dumler and Mr. Rick Haasch for providing technical assistance and answering my constant questions.

Special thanks are due to my fellow students and colleagues, especially Dr. Z. Zhang, Dr. Z. Xing, and Dr. C. Zhang, each of whom has contributed to my overall understanding of this work through group discussions and experimental assistance.

I am deeply indebted to the United States Air Force (both figuratively and literally) for paying my tuition and enabling me the opportunity to pursue this degree. My program managers, Captain Tom Neu and Captain James Ulman have helped greatly by answering specific questions regarding both this thesis and Air Force requirements in general. Fellow AFIT students and the cadre at ROTC Detachment 190 are owed thanks for reminding me why I was here and keeping me in contact with a military environment.

Last but not least, I need to thank my family and friends for believing in me and helping me to believe that, despite my constant protests to the contrary, I would eventually graduate. Thanks also to my brother, Mike, for taking the time to proofread this document and make sure all the *i*'s were dotted and *t*'s were crossed.

This work was supported by the Federation of Advanced Materials Industries.

Table of Contents

List of Tables

List of Figures

Chapter 1

Introduction

Over the past fifteen years or so, the use of carbon fiber reinforced composites (CFRC) has grown substantially. These materials offer the advantageous properties of high strength and stiffness with substantial weight savings over more conventional materials such as aluminum alloys. Furthermore, composite materials have the unique benefits of tailorability. In other words, it is possible to tailor their properties to meet the specific requirements of a particular application. The combination of these characteristics make CFRC an ideal choice for use in advanced aerospace structures and are the driving force behind their increased employment in recent years [1].

Despite the fact that carbon fiber composites have found increasing application, many aspects of these materials are still not clearly understood. One of the fundamental questions remaining concerns the adhesion between fiber and matrix. In order to utilize the strength and stiffness of the reinforcing fibers, it is essential to optimize the bond between the polymer resin matrix and the fiber surface. Since the early 1960s, the issue of adhesion between fiber and matrix has been the subject of continuing research. In particular, many techniques for increasing the strength of the bond between graphite fibers and epoxy adhesives have been proposed and tested, both in the laboratory and in service. Additionally, a number of models have been advanced in the hopes of explaining why some of these techniques work better than others. Such models explain adhesion phenomena by suggesting some mechanism which attempts to relate the interplay of the three interactions known to exist across the interface: mechanical interlocking, chemical binding, and weak attracting forces such as dipole-dipole, van der Waals, and electrostatic

interactions [2]. However, none of these models has proven adequate to sufficiently explain the extent of these interactions. So, the question remains unanswered.

Another concern relating to the issue of fiber/matrix adhesion is the fact that as aircraft become more expensive, their expected service life increases as well. Hence, the question of fiber/matrix adhesion under conditions of cyclic loading takes on added importance as these materials will be expected to see more and more cycles in their lifetime. Unfortunately, fatigue testing of this interface cannot be easily done. The main problem with attempting an exhaustive study of the graphite/epoxy interface in fatigue lies in the frail nature of the fibers. Because of the properties of the fibers themselves, popular single fiber tests, like the fiber pull-out test, are not possible for conditions of cyclic loading. As a result, the only fatigue testing done to date has focused on composite laminates as a whole, leading to problems in interpretation from complicating factors such as fiber volume fraction, laminate orientation, etc., and preventing a detailed analysis of interfacial fatigue resistance. In an attempt to avoid these complicating factors, this thesis makes use of the newly developed flexural peel technique to investigate fatigue crack growth along the graphite/epoxy interface, taking pyrolitic graphite as the substrate to model the carbon fiber (CF) surface. This research has been focused on the correlation between fatigue behavior, chemistry, and morphology of the graphite/epoxy interface.

1.1 Overview of Thesis Research

Characterization of the interface between graphite and epoxy is very complex, involving surface chemistry, physical chemistry, organic chemistry, adsorption and chemisorption, surface structure, and microstructure. Optimization of interfacial adhesion, is likewise complex and always involves some type of modification of the CF surface. In this thesis, common techniques of surface treatment of graphite fibers for adhesion to

polymeric adhesives are surveyed first, including both oxidative and non-oxidative techniques and etching and coating methods. Also discussed are some recent studies in which surface modification techniques were applied to pyrolitic graphite as a means of modeling the CF surface. Chemical and mechanical effects from plasma etching of pyrolitic graphite edge surfaces for different lengths of time, as well as the effects of subsequent heat treatments designed to restore the original surface chemistry are examined. The fatigue crack growth rates along the interface between an epoxy adhesive and graphite substrates following these surface treatments are then measured as a function of strain energy release rate. Results of these tests are explained in terms of both surface morphology and chemical interactions based on SEM, XPS, and surface profilometry analyses.

Chapter 2

Modification of CF Surfaces for Adhesion to Epoxy Resins

The strength of the interface in graphite/epoxy composites has long been known to be of critical importance to the overall mechanical properties of such materials. An abundance of literature is available which examine the parameters affecting adhesion between graphite fibers and polymer matrix resins. Much of this literature is devoted to surface modification techniques of CF to improve adhesion and can be broken down into two broad categories: (1) oxidative techniques, in which the focus is the addition of oxygen-containing functional groups to the surface of the graphite; and (2) non-oxidative techniques, in which other methods of adhesion improvement are sought, such as surface roughening or coating with an organic layer more likely to bond with the polymer resin. Obviously, these two categories are not mutually exclusive, as many techniques aimed at adding oxygen to the CF surface also roughen the material. Also, within these two categories are a number of subdivisions including, liquid phase oxidation, gas phase oxidation, and anodic etching. These categories and subdivisions will be discussed in the following sections, with special emphasis on how such techniques have advanced the understanding of the important parameters affecting interfacial adhesion. Finally, surface treatments applied to the basal and edge surfaces of pyrolitic graphite substrates to model the CF surface[3-9] will be discussed as its own category.

2.1 Oxidative Techniques

An extremely inert material, graphite does not bond very well to epoxy matrices[10,11]. Consequently, it has been suggested that the addition of oxygen-containing functional groups to the fiber surface would enable strong bonds to develop

across the fiber/matrix interface and thereby improve interfacial adhesion. In fact, the introduction of oxygenated groups at the fiber surface appeared to be an attractive route since the earliest stages of CFRC development. In 1973, McKee and Mimeault published the first review of work on the oxidation of carbon fibers[12]. Subsequent research[13-15] has revealed that carbon can be oxidized both by liquid and gas phase techniques. Both types of oxidation are commonly used.

Since a comprehensive examination of each method of carbon fiber oxidation is beyond both the scope and interest of the current study, these techniques are discussed in the following sections on a general level, from the perspective of how they relate to an overall understanding of controlling factors of adhesion at the graphite/epoxy interface .

2.1.1 Liquid Phase Oxidation

A wide range of oxidation agents has been used including nitric acid, hydrogen peroxide, sodium hypochlorite, and acidic potassium permanganate. With each of these reagents, the basic procedure for oxidation remains the same. Fibers are treated in solutions of varying concentration and temperature for a specified amount of time. Depending on the type of oxidizing agent, type of fiber, exposure time, and process temperature, these treatments can have varying effects on both morphology and surface functionality.

Among the oxidizing agents used, nitric acid is the most common. Working with nitric acid treatments (60% for 24 hr at the boiling point), Herrick and co-workers[16,17] found a surface area increase from 1 to 136 m^2/g with a corresponding 12% reduction in weight, while oxygen content (measured in terms of carboxyl groups) showed a ten-fold increase. In the same experiment, interlaminar shear stress (ILSS) was also found to increase from 4400 to 5930 psi with surface treatment. Prolonged exposure to nitric acid

was found to result significant decreases in fiber strength, likely due to the continued etching of the fibers by the acid. At the same time, the use of more dilute acid was ineffective in increasing surface functionality. Fitzer and co-workers[18] and Cziollek[19], oxidized type I and II PAN-based carbon fibers by refluxing with 65% nitric acid followed by extracting in water and drying at 150°C for 48 hours. They found that for both types of fibers, surface oxygen content increased with increasing treatment time. Hamin et al.[20] used 65% aqueous nitric acid solutions at 120°C for 5 hours followed by cleansing in water and drying in vacuum at 150°C for 1 hour to oxidize carbon fibers. Results from their work indicated that surface treatment produced fibers with increased concentrations of surface oxygen and no significant loss of mechanical properties. The work of Bahl and co-workers[21], demonstrated that treating polyacrylonitrile (PAN) based carbon fibers with 50% nitric acid for 50 minutes provided the best results. This treatment produced fibers which had undergone some surface smoothening and had significant increases in oxygen-containing functional groups at the surface. Longer treatment times resulted in higher oxygen concentrations, but the overall mechanical properties, such as tensile strength, suffered with further exposure.

Bansal and Chhabra[22] and Bansal et al.[23], oxidized PAN-based carbon fibers in mild oxidizing agents such as aqueous solutions of hydrogen peroxide and potassium persulfate. Oxidation was performed by immersing the fibers in closed bottles of these solutions for 24 hour periods. Both types of treatment resulted in increased concentrations of surface oxygen-containing groups that were proportional to the amount of fiber etching. Using a 15% peroxide solution near boiling for 14 hours, Yip and Lin[24] oxidized several different types of carbon fibers. Their findings included appreciable rises in surface roughness and oxygen content of the fibers as well as increases in transverse tensile strength (TTS) of their resulting composites. These increases were attributed to the

formation of micropores, cracks, etch pits, lamellar oxide layers, and elimination of trapped carbon atoms and weakly absorbed oxygen.

2.1.2 Anodic Etching

A specialized form of liquid phase oxidation, anodic etching makes use of the excellent conductive properties of carbon fibers. In anodic etching processes, the carbon fibers act as an electrode across which a bias may be passed. Using dilute concentrations, a wide variety of electrolytes may be used, including both alkaline and acidic media. Since the anodic etching process is quite mild (resulting in less than 2% weight loss of the fibers), no significant change in the surface area of the fibers occurred. Nevertheless, numerous studies have been done which indicate that this technique can produce significant changes in the amount and type of functional groups on the fiber surface.

A number of investigations were done in the 1980s by Sherwood and co-workers[25-29] which systematically studied the effects of various electrolytes and anodizing potentials on the chemistry of CF surfaces. Using concentrations as low as 10% electrolyte in aqueous solution, they found that the number of surface oxygen-containing groups increased with increasing potential. Applied voltage not only affected the amount of functional groups, but it had a direct effect on the type of surface species as well. At lower potentials, ketones dominated the surface, while -C-O concentration increased with increasing potential. Results also indicated that acidic electrolytes produced more dramatic changes than alkaline solutions at the same potential and that the majority of functional groups were added at corner and edge sites, rather than along basal surfaces. Similar work with sulfuric acid, sodium hydroxyl, and ammonium carbonate done by Verbist and Lefebvre[30] supported these conclusions. In these studies, applied anodic potentials were

kept below 2.0V to avoid strong fiber damage, which is often accompanied by the evolution of CO and CO_2 during treatment. Treatment times of 1 minute at the highest applied voltage produced the greatest increases in functionality for all three electrolytes. Also, the relative concentrations of functional groups at different potentials were much like those found by Sherwood.

More recent studies by Wang and Sherwood[31,32] have attempted to relate the effects of electrochemical oxidation of carbon fibers to their reactivity with polymeric resins. These studies show that fibers treated in this manner react chemically with resin materials, but attempts have not yet been made to quantify these reactions in terms of adhesion strength between fiber and matrix nor with transverse strength properties of composite laminates as a whole.

Baillie and Bader[33] performed a comprehensive investigation into the effects of anodic oxidation on adhesion to epoxy matrices for PAN-based carbon fibers in an ammonium-bicarbonate electrolyte at various current densities. Results indicated that debonding stress increased with potential up to $25C/m^2$, after which it leveled off. Strength increases were attributed to the removal of a weakly-bonded surface layer on the fiber, thereby making it possible for acid groups to anchor to the fiber surface. As the concentration of these acid groups increased, the failure mode changed from one of frictional sliding across the interface (no treatment) to the breaking of chemical bonds between the fiber and matrix (optimal treatment). The strength plateau after $25C/m^2$ was attributed to a saturation of active sites on the graphitic surface.

2.1.3 Gas Phase Oxidation

Early attempts at gas phase oxidation of carbon fibers made use of air or oxygen gas at high temperatures. Molleyre and Bastic[34] oxidized PAN-based carbon fibers in air

at 500°C and studied the resulting fiber characteristics for comparison with untreated fibers. Surface area, surface roughness, and pore size all increased with treatment, and correlation was made between the increased surface roughness and improvements in composite shear strength. However, this study also revealed that when the same treatment was performed in CO_2 rather than in air, the resulting fiber surface was smoother and the pore sizes were smaller than in the untreated fibers. Clark et al.[35] also reported a marked increase in surface rugosity through the formation of pits and striations when fibers were oxidized in air. The interlaminar shear strength (ILSS) of composite materials made from HM carbon fibers with this treatment increased from 20 to 58 MPa.

Yip and Lin[24] pre-soaked a variety of types of CF in concentrated sulfuric acid at boiling point for 1 hour followed by heating in a muffle furnace for a period of hours, with exact time depending on fiber type. Oxidation appeared to take place preferentially at surface defects, cracks, bumps, and pits. Both oxygen content and TTS increased with treatment, although the authors believed chemical bonding between fiber and matrix contributed only to a minor extent in adhesion.

Oxidation of PAN-based CF was accomplished by Bansal and Chhabra[22] by soaking the fibers in water and bubbling in an oxygen/3% ozone mixture for 6 hours. Reportedly, this treatment enabled oxygen to be chemisorbed to the surface and resulted in increased fiber surface area with only a 6% weight loss. However, attempts were not made to correlate these results with interfacial adhesion.

Out of a need for an alternative to both high temperature gas phase oxidation as well as to liquid phase oxidation came the concept of cold plasma oxidation. The idea that gas plasmas could effectively be used to modify the surface of carbon fibers first began to take shape in the patent literature in the early 1970s[36-39]. The techniques entailed in these patents make use of oxygen-containing gases such as NO_2, O_2, SO_2, CO_2, NO, H_2O, and

air plasmas to oxidize carbon fibers. By the mid-1980s, studies in the literature began to appear which demonstrated that these oxidizing plasmas were able to significantly functionalize a surface.

Mujin and co-workers[40] used cold O_2 plasma to treat bundles of 1000 fibers at a time by passing the bundles into the plasma at a constant velocity. Various techniques were then used to characterize both the physical and chemical properties of the resulting fibers. The shear strength (ILSS) of carbon fibers reinforced composites made from these fibers was measured and found to increase by almost 70% over those composites made from untreated fibers. Improvements were attributed to three areas. First, there was no appreciable loss of fiber strength as a result of the treatment. Second, increased surface roughness enhanced mechanical interlocking at the interface. Third, an increase of oxygen-containing groups at the fiber surface, mainly in the form of carboxyls and ketones, improved wettablilty and reactivity of the CF towards epoxy resin. Allred and Schimpf[41] obtained similar results using CO_2 plasmas on high modulus carbon fibers. Treated fibers showed large increases in surface functionality mainly in the form of hydroxyl, ketone, and carboxyl groups. Increases in composite shear strength were also noted as functions of the increased surface oxygen.

In working with air plasma, Xie and Sherwood[42,43], demonstrated that microwave plasmas were also an effective CF surface treatment. They noted that exposure to air plasmas caused increases in surface oxygen-containing groups as well as increases in nitrogen functionalities. Furthermore, treatment affected only the *surface* chemistry of the fibers, while the bulk structure was unchanged. Treatment times of less than five minutes produced best results, with oxygen increases attributed to the added presence of C-OH, C-O-C, and -C=O groups. Longer treatment times proved ineffective in producing more functionality and resulted in degradation of fiber strength. Sherwood also noted that there

exists a critical time for both O_2 and air plasma treatments after which some functionality will be lost and fiber damage will occur. Similar results in working with air plasmas were obtained by Jones et al[44,45]. They concluded that air plasma treatments resulted in increased surface oxygen groups, which could improve adhesion to matrix materials. The same work showed that the etching effect of argon plasmas led to a large number of free radical sites on the CF surface. When the treated fibers were then exposed to air, these sites reacted with atmospheric oxygen and nitrogen to produce large increases in surface functionality. However, this study did not attempt to relate increased oxygen levels with any composite properties. Correlation between surface oxygen groups and fiber matrix adhesion were also obtained by Allred and Stoller for Kevlar fibers[46] and Zang et al.[47] for PAN-based carbon fibers.

In a study quoted extensively, Drzal and co-workers[48] studied the plasma treatment of PAN-based fibers in air. They suggested that surface treatments designed to promote adhesion of CF to epoxy matrix materials operate through a two-part mechanism. First, a weak outer layer initially present on the fiber surface is removed by the surface treatment. Second, surface chemical groups are added to the fiber surface which could increase interaction with the matrix chemically, leading to improved fiber matrix adhesion. Drzal also claimed that the increases in surface area caused by many treatments do not have an important effect on the overall adhesion between fiber and matrix.

In a recent study by Drzal [49], attempts were made to correlate the amount of surface functional groups with adhesion at the fiber/matrix interface. Results seemed to indicate that chemical bonding between matrix materials and these functional groups was not the dominant factor in adhesion (approximately a 20% effect).

2.2 Non-Oxidative Techniques

While treatments involving the addition of oxygen to the surface of carbon fibers have enjoyed the dominant position both in service and in research, many alternative techniques have taken on increasing importance over the past 10 years. With the exact mechanism by which adhesion between CF and epoxy occurs still not fully understood, nonoxidative surface treatments have arisen in the hopes of providing improved adhesion cheaper, faster, and/or more reliably than the established techniques. Some of the more popular new treatments are mentioned below.

2.2.1 Whiskerization

The process of whiskerization involves a nucleation and growth process of very thin, very high strength materials such as silicon carbide, titanium oxide, or silicon nitride on the fiber surface perpendicular to the fiber axis. Milewski and co-workers[50-52] first used the concept of whiskerization to grow a uniform coating of silicon carbide whiskers onto the surfaces of carbon fibers via a chemical vapor deposition process at about 1400°C. They claimed that this process enabled them to increase the shear strength of a carbon composite by more than 4 times over the shear strength of those made from untreated fibers. However, the use of silicon carbide presented some major problems. The material is very abrasive, much more dense, and has a different coefficient of thermal expansion than carbon. Furthermore, the very high temperatures at which this process had to occur made it a very unattractive option for industrial uses.

Baker and Downs[53] proposed an alternative to circumvent these problems by growing carbon nanofibers from the surfaces of both PAN and pitch-based carbon fibers at relatively low temperatures (650°C). This process involved the use of a metal catalyst, introduced to the fiber by means of a soluble salt followed by several calcination and

reduction steps to produce discrete metal particles on the fibers. When exposed to a gaseous hydrocarbon/hydrogen mixture at 650°C, these particles acted as catalysts from which the nanofibers were grown. Treatment in this manner produced very large increases in surface area of the fiber from about $1.0m^2/g$ in the untreated state to as large as $300m^2/g$ when completely covered by nanofibers. Mechanical tests on composite materials made from these treated fibers indicated that shear strengths as much as 4.75 times larger than untreated samples were possible.

2.2.2 Coating Methods

Thin coatings of organic polymeric materials (finishes or sizings) are another method which have been employed to improve interfacial adhesion. Though often applied primarily as a protective coating, fiber finishes can also improve fiber surface reactivity and wettability with polymer resins. Cziollek et al.[19] coated PAN-based carbon fibers which had been pre-oxidized in 65% nitric acid with a liquid epoxy and a liquid diamine. They found that this procedure produced increases in the TSS of the resulting composites from 30 to 50% over the TSS of untreated specimens. The use of several alternating and block co-polymers has also proved to be successful in improving adhesion with PAN-based carbon fibers[54].

Drzal et al.[55] studied the effect of fiber finishes with respect to adhesion with epoxies and concluded that the coating had a two-fold effect. First, there was an increase in interfacial strength between fiber and matrix. Second, the mode of failure at the interface was altered from growth of an interfacial crack between fiber and matrix to that of a matrix crack perpendicular to the fiber axis. Drzal concluded that the finish reacted with the matrix material to create a brittle "interphase" which contained a lower concentration of curing agent than the bulk epoxy (Figure 2.1). This interphase region

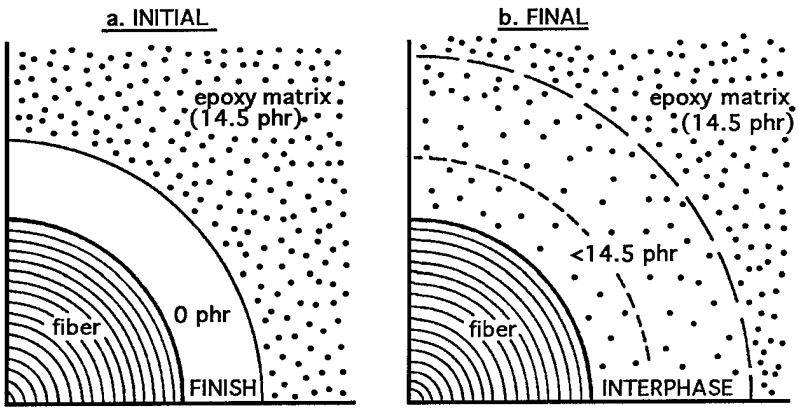

Figure 2.1: Schematic diagram of the interphase region: (a) initial bonding; (b) after final cure [55]

was able to promote better stress transfer between the fibers and matrix, but because of its low fracture toughness (a consequence of the depletion of curing agent in the region), the failure mode changed from interfacial to matrix cracking. These observations were confirmed by Okhuysen et al.[56], who saw a similar change in failure mode of fibers coated with either diglycidyl ether or bisphenol A.

Attempts by Commercon and Wightman[57] to coat pitch-based carbon fibers using organic gas plasmas were not successful in improving interfacial adhesion. They found that treatments with methane, ethylene and trifluoromethane led to a decrease in debonding strength between the fibers and PES resin. The decrease in adhesion was attributed to these films acting as a "weak boundary layer." Further studies with epoxy resins yielded the same conclusions.

2.2.3 Other Methods

There are two techniques which need to be included under the heading of "other techniques" used to modify carbon fibers for adhesion. The first of these is the vapor deposition of pyrolitic carbon and certain metal carbides[58-60]. These materials have been

deposited onto the surfaces of carbon fibers both to improve adhesion as well as to improve resistance to oxidation. Employed most often when dealing with ceramic or metal matrices, this technique is best suited for stabilizing the properties of the fiber under exposure to high temperatures or corrosive environments. As such, vapor deposition has not seen much use with polymer based composites.

Another technique which as yet has not seen abundant use is the modification of carbon fibers with fluorinated etching plasmas. Commercon and Wightman[57] have recently demonstrated that tetrafluoramethane (CF_4) plasma treatments can enhance the adhesion of carbon fibers to epoxy resins. The authors point out, however, that the adhesion improvements are a consequence of the etching effects of the plasma rather then a chemical effect. Supporting the conclusions of Drzal et al.[48], they argue that their results emphasize the importance of the removal of a "weak boundary layer," as the dominant effect in the fiber-epoxy adhesion.

2.3 Using Pyrolitic Graphite to Model the CF Surface

Because the structure of carbon fiber surfaces is complicated and often does not show a homogeneous structure, it can be extremely difficult to characterize the relationship between the structure of CF surfaces and the species of chemical groups added by surface treatments. Furthermore, the inability to sufficiently characterize this surface makes the determination of the mechanism responsible for the improvement of interfacial adhesion a controversial subject. In response to these problems, an innovative method for modeling the surface of carbon fibers has been introduced and investigated by Nakahara and co-workers over the past five years. They have studied the nature and relationships mentioned above by using basal and edge surfaces of pyrolitic graphite (PG) as a model of the CF surface. The scope of their investigations falls into three areas: (1) anodic oxidation and its

effects; (2) plasma irradiation and its effects; and (3) polymer/PG edge surface interface characterization.

Studies on the effects of anodic oxidation involved the use of different electrolytes as well as different oxidizing potentials [3,4]. Characterization of PG surfaces both before and after treatment was performed by means of laser Raman spectroscopy as well as x-ray photoelectron spectroscopy. It was determined that by anodic oxidation, hydroxyl groups (C-OH) are added to edge surfaces of PG. According to the authors, it is these hydroxyl groups which are capable of bonding covalently with epoxy to improve adhesion. Carboxyl groups (C=O), associated with the destruction of the surface structure, were added to the basal surfaces. Because these carboxyl groups were added to the surface only when a degradation of the crystalline order occurs, they are not believed to improve adhesion with epoxy resins. Thus, the edge surface is considered to play the more important role in improving adhesion. Comparing the effects of acidic versus alkaline electrolytes, two general conclusions were reached. First, the depth of oxidation in acidic electrolytes may be as much as 40nm, whereas with basic solutions oxidation is limited to the surface layer at all treatment levels. Second, the use of acidic electrolytes causes a great deal of destruction of the PG surface, both at edge and basal sites. Alkaline electrolytes, even at high levels of treatment ($5000C/m^2$), do not cause destruction of the surface structure. This relationship between type of added functional group, depth of oxidation, and amount of surface destruction is shown in Figure 2.2.

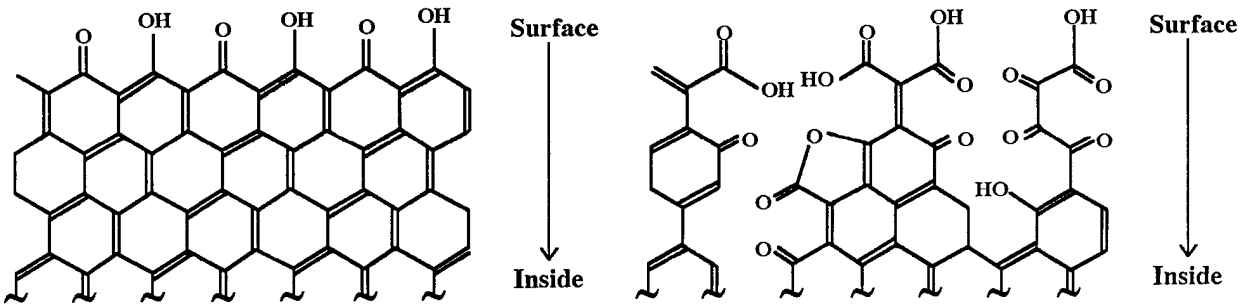

(a) (b)

Figure 2.2: Relationship between functional groups added to edge surfaces: (a) -OH; (b) -COOH [5]

Building on the information obtained in characterizing PG surfaces modified by electrochemical oxidation, Shimizu and co-workers[5] attempted to relate structural changes caused by these treatments to the interfacial debonding strength (IFDS) between epoxy and PG edge surfaces. For both the acid and alkaline electrolytes, IFDS initially increased with anodic potential from about 4MPa to a maximum of 9MPa, but dropped to zero for a potential of 50,000C/m^2. The increases in strength were attributed to increases in hydroxyl formation on the PG surface, while the drop-off in IFDS was attributed to the addition of carboxyl groups and a subsequent destruction of the surface order.

In a related set of experiments, Nakahara and Sanada [6] turned their attention to characterizing the effects of an oxygen plasma treatment on PG surfaces. Characterization was once again carried out using XPS and laser Raman spectroscopy. It was found that plasma treatment increased oxygen content on both basal and edge surfaces, and that on both surfaces, the increased oxygen content appeared to come in the form of carbonyl groups as opposed to -O- type groups. There were two primary differences between treated basal and edge surfaces, however. Although oxygen content increased on both surfaces, it did so at a much faster rate for the edge areas, leading to the conclusion that the edge surface is of greater importance in optimizing adhesion properties. Also, the plasma

treatment caused a slight destruction of the basal surface while no marked destruction occurred on the edge surface with treatments as long as 240 minutes. Schematically, the effect of plasma irradiation on these two surfaces is shown below in Figure 2.3. Note that the plasma seems to preferentially attack defects on the basal surface whereas the net effect of treatment on the edge surface appears to be the removal of a disordered layer.[7] It may be that the removal of this disordered layer, which is introduced to the sample during specimen preparation, is akin to the similar phenomena of outer boundary removal described by Drzal et al.[48] as part of the two part mechanism for adhesion at the graphite fiber/epoxy interface.

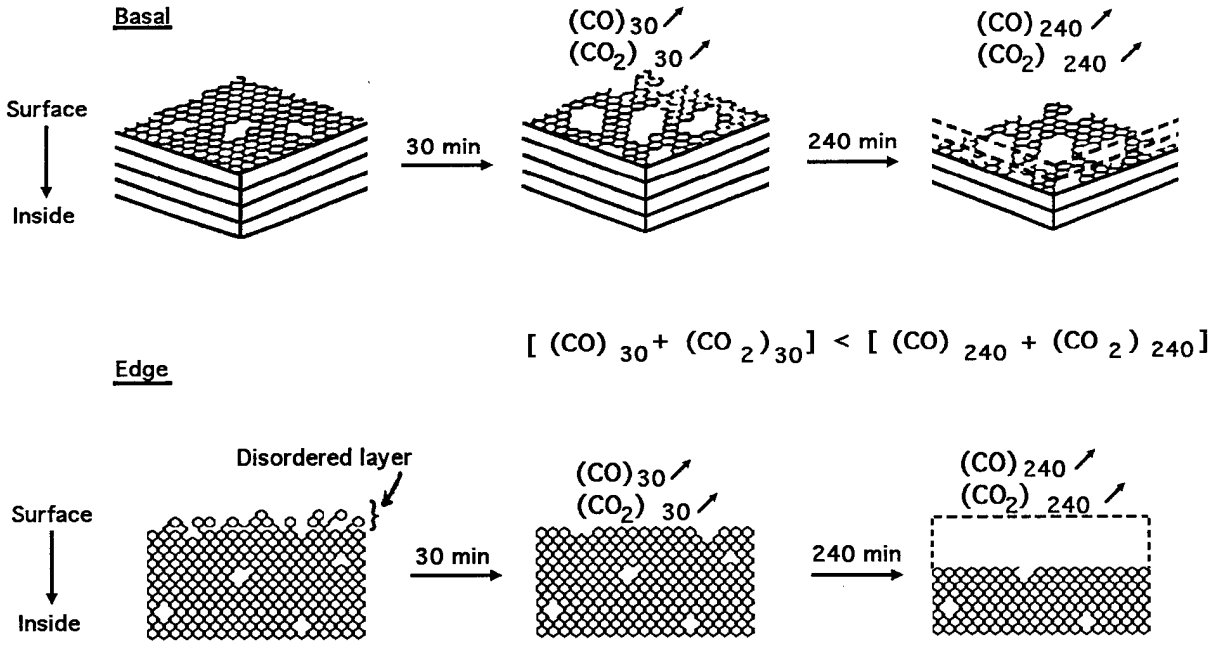

Figure 2.3: Diagram of the structural changes of basal and edge surfaces by oxygen plasma treatment. (CO) and (CO_2) represent the gas evolved after plasma treatments of various times[6].

2.4 Summary

Judging by the number of studies performed on the subject, the nature of adhesion between graphite fibers and epoxy resins is at the same time both a complex and important

area of research. The ability to modify the surface of carbon fibers for improved adhesion is well documented. What is not well understood, however, are the factors which control this adhesion. Without this fundamental understanding, attempts to optimize surface treatments will continue to run on a trial and error basis. Most researchers agree that both chemical effects (through the addition of reactive functionalities) as well as physical effects (in terms of mechanical roughening) play a part in adhesion at this interface. As yet, though, no one has been able to conclusively demonstrate the magnitude of their respective roles. With the use of pyrolitic graphite to provide a simplified model of the CF surface, it may be possible to successfully answer this question and determine the best way to optimize interfacial adhesion and fatigue resistance of the graphite/epoxy interface.

Chapter 3

Experimental Procedures

3.1 Materials

Pyrolitic graphite was selected as the model substrate in this study for two reasons. First, the clean, ordered, homogeneous structure of PG made it possible to avoid difficulties in the characterization of the surface which are often encountered when using carbon fibers, due to the complex structure and non-homogeneous surface of such fibers. Pyrolitic graphite also has excellent strength properties, making possible the analysis of the carbon/epoxy interface under conditions of cyclic loading without having to use an entire composite laminate. Because bulk graphite samples could be used in lieu of whole laminates, it was also possible to avoid complications from such variables as fiber volume fraction and degree of orientation.

3.1.1 Pyrolitic Graphite

The pyrolitic graphite used was provided by the Advanced Ceramics division of Union Carbide Corporation, Cleveland OH. Pyrolitic graphite is a high purity material composed of carbon atoms arranged in parallel layers of adjacent hexagonal rings. Figure 3.1 shows a sketch of a typical PG sample (with dimensions noted) as received from the vendor for this study. As shown in the figure, the "a" direction is parallel to the deposition surface (and therefore to the basal planes as well), while the "c" direction is perpendicular to the deposition surface.

The impurity content in the bulk graphite is very low, as seen in Table 3.1. The ash content ranges between .001 and .003% weight, with the majority of its impurity content consisting of silicon (50%). Crystallite size varies between 50 and 5000Å, while the

spacing between layers of adjacent basal planes is approximately 3.4Å. Degree of orientation is very high with the ratio of crystallites having basal planes parallel to the deposition surface to those oriented normal to the deposition surface falling between 100:1 and 1000:1.

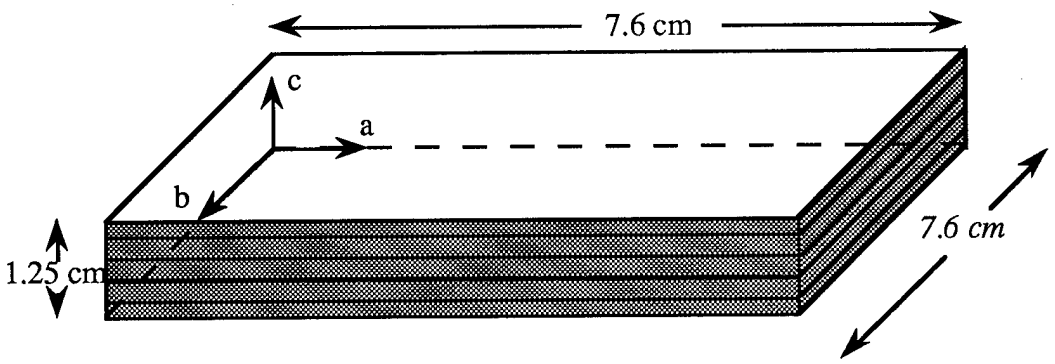

Figure 3.1: Schematic of pyrolitic graphite sample

Table 3.1: Impurity content of pyrolitic graphite[61]

Element	Weight %
B	0.001
Ca	0.0001
Al	0.0001-0.001
Mg	0.0001
Si	0.0001-0.001
Fe	0.0001
Cu	0.0001
Ti	0.0001
V	trace

As PG is a highly anisotropic material, property data is usually reported for both the basal and edge surfaces ("ab" and "ac" planes), when applicable. Since the edge surface is of most interest for the purpose of adhesion to polymeric materials and was the surface used in this study, only those relevant properties associated with the "ac" plane are reported here.

Table 3.2: Properties of pyrolitic graphite ("ac" plane)[61]

Density	2.20	g/cm^3
Modulus of elasticity	27.6	GPa
Ultimate tensile strength (load applied//to "a" direction)	68.9	MPa
Ultimate strength in bending (load applied//to "b" direction)	103.4	MPa

3.1.2 DP-420 Epoxy

The adhesive system chosen for this study is a two-part, room temperature-curing epoxy made by 3M (3M designation DP-420) and toughened by unspecified additives. The basic ingredients as disclosed by the vendor are listed in Table 3.3 below. The material properties for this epoxy were determined earlier and procedures detailing the determination of these properties have been discussed elsewhere[62]. Relevant mechanical properties are listed in Table 3.4 below.

Table 3.3: Ingredients of DP-420 epoxy

Ingredient	Weight %
Polymeric amine	50-60
Epoxy resin—N.J. Trade Secret	20-30
Epoxy resin	1-10
Amorphous silica	1-10
2,4,6-tri((dimethylamino)methyl)phenol	1-10
Catalyst	1-10

Table 3.4: Properties of DP-240 epoxy

Elastic modulus	2.25GPa
Tensile yield strength	30 MPa
Ultimate tensile strength	35 MPa
Shear yield strength	17 MPa
Ultimate shear strength	20 MPa
Poisson's ratio	0.40

3.2 Surface Characterization

3.2.1 Specimen Preparation

Pyrolitic graphite samples were received from Advanced Ceramics as plates with dimensions as shown in Figure 3.1. From the bulk sample, specimens were cut to desired dimensions with a diamond tip blade as shown in Figure 3.2, where the dashed lines indicate the cutting plane.

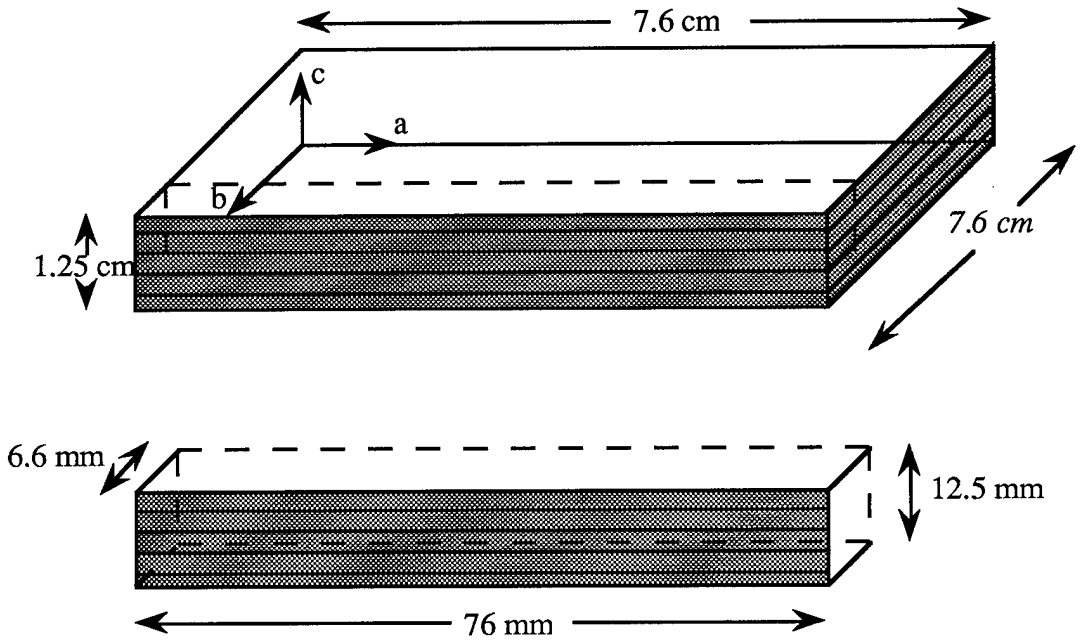

Figure 3.2: Specimen geometry (Shown as cut from received graphite)

Surface morphology samples were made by sectioning the above plates into smaller dimensions (approximately 12.5mm x 12.5mm x 6.6mm thick).

The surface preparation for all specimens was the same. Immediately after sectioning, samples were rinsed twice in an ultrasonic bath using de-ionized water and then dried with bursts of compressed air. Then, edge (shaded) surfaces were ground flat and rough polished using 400 and 600 grit silicon carbide abrasive paper. Polishing was accomplished by changing polishing direction by 90° when moving to the finer grit paper.

Polishing then continued until the scratch marks from the 400 grit paper were no longer visible on the sample. In addition, samples were directionally polished so that the final polishing direction was 90° to the anticipated direction of crack growth (i.e. on the edge surface, in the "c" direction of Figure 3.2). The samples were then ultrasonically rinsed three times in acetone and three times in de-ionized water. After the rinsing process, compressed air was used to dry the samples. The graphite was then allowed to finish drying overnight.

3.2.2 Plasma Treatment

In order to perform the dual task of roughening as well as functionalizing the graphite surface, radio frequency (RF) glow discharge plasma etching was used. Specimens were etched with oxygen plasma in a Texas Instruments, model ASD-4, planar plasma system with the following operating conditions: a process pressure of 500mTorr, a process temperature of 20°C, and a power setting of 300W. Treatment times were set at 5, 10, 15, and 30 minutes.

3.2.3 Heat Treatment

After plasma treatment, some samples were subjected to a heat treatment designed to remove the functionality from the surface while retaining the etched surface morphology. Heat treatment was accomplished in an induction heating furnace at the Center for Materials Processing, University of Illinois at Urbana-Champaign. Specimens were heated to 1000°C at a vacuum of approximately 10^{-7}torr for 1 hour. After cooling to room temperature, the chamber was back-filled with hydrogen to prevent oxidation of the surface. Similar treatments designed for removing the functionality of carbon fibers have been performed and analyzed by Hammer and Drzal[63] and Yip and Lin[24].

3.2.4 Surface Chemistry

For a more detailed understanding of the differences in surface chemistry produced by various treatment times, the specimens were examined using x-ray photoelectron spectroscopy (XPS). Analyses were performed in vacuum at room temperature using Mg K_a x-rays at 1246eV as the photoexitation source. The x-ray source and argon ion source were mounted at an angle of approximately 45° from the surface of the specimens. Photoelectrons generated from the surfaces were focused on the entrance slit of a hemispherical energy analyzer. A pass energy of 180eV was used to scan the surface for general elemental analysis while more detailed analysis of specific peaks was accomplished with a pass energy of 36eV. Spectral data were recorded and analyzed by computer to give surface composition.

3.2.5 Surface Morphology

3.2.5.1 Surface Profilometry

Untreated, plasma treated, and heat treated specimens were subjected to surface profilometry analysis to determine the samples' arithmetic average (AA) roughness, defined as the root mean square deviation from the mid-line of the surface. Profilometry was conducted on a Dektak^{3}ST surface profiler. Scans were taken along the direction of expected crack growth (i.e. on the edge surface, in the "a" direction; see Fig. 3.3 below). Each scan was approximately 50μm in length and took 6 seconds to complete, providing for 1000 data points per scan. Arithmetic average roughness was found for samples of each treatment time. A minimum of five scans were taken for each treatment time.

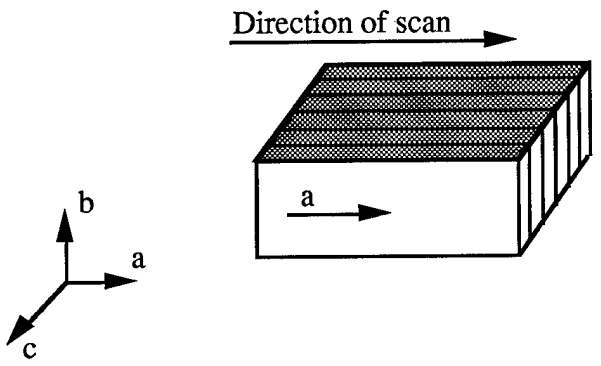

Figure 3.3: Scan direction for surface profilometry analysis

3.2.5.2 SEM Observation

The surface morphology samples described above for treatment times of untreated, 15min, and 30 min were subjected to surface observation in SEM* . The study focused on the morphology of the graphite surface along the "ac" plane with emphasis placed on the differences caused by various treatment times. Specimens were coated with Au/Pd for 180 seconds prior to SEM analysis in order to ensure that no charging would occur on the surfaces during observation. Coating operations were performed in a Polaron SEM sputter coating system at a process pressure of approximately $1.8x10^{-1}$mbar and an accelerating voltage of 800V. These parameters ensured a deposition rate of approximately 2Å/s. Specimens were observed at a variety of angles including no tilt, 30° tilt, and 90° tilt with respect to the plane of interest in order to fully characterize their morphology.

3.3 Crack Growth Experiments

3.3.1 Sample Preparation

Crack growth specimens were prepared in the same manner as described above for the surface morphology samples. Samples were cut to dimensions shown in Fig. 3.2, and

* Zeiss, Model 960

directionally polished as before. In addition, one of every two samples was cut to approximately 2/3 its original length, for use as the top half of a flexural peel specimen (discussed in Sec. 3.3.2). Plasma treatment times were either 15min or 30 min, with the operating parameters remaining at 300W, 500mTorr and 20°C. Crack growth tests were performed on polished and etched samples, as well as on specimens heat treated to restore the original surface chemistry.

3.3.2 Specimen Fabrication and Geometry

Specimens used for crack growth experiments were made to conform to a flexural peel (FP) geometry. Basically, this geometry consists of three layers made of two different materials. The outer layers were made of PG, and the inner layer was epoxy adhesive. Figure 3.4 shows the geometry and appropriate dimensions of the FP specimens used in this study.

The procedure outlined below for making the FP specimens was used for samples of each treatment condition. First, a strip of adhesive tape was applied to the bottom beam over the bonding surface including approximately 10mm of the overlap area. This tape would later serve to produce a pre-crack region between the adhesive and the lower graphite layer. Next, epoxy adhesive was generously applied to both bonding surfaces. Two brass shims were then placed on the lower graphite layer, one at the "rear" of the specimen and the other in the pre-crack region. The purpose of these shims was to ensure a constant thickness in the adhesive layer. Finally the two halves of the FP specimen were brought into contact and clamped together by clips spaced evenly around the perimeter of the sample. Specimens were cured in this position for a period of no less than five days, after which the clips were removed and excess epoxy around the edges was ground away using 600 grit abrasive paper.

3.3.3 Experimental Technique

Fatigue crack growth experiments were performed on the Flexural Peel specimens under displacement-controlled conditions using a sinusoidal waveform at a frequency of 10Hz and a load ratio of 0. Testing was accomplished in room air (22°C; 55% relative humidity) on a testing apparatus specifically designed for FP specimens, as shown in Figure 3.5. The initial crack was formed in the specimen by overloading the region containing the adhesive tape until a crack developed. Due to the geometry of the sample and placement of the load, this procedure ensured that the initial crack would in fact form along the lower interface between the bottom graphite layer and the epoxy adhesive.

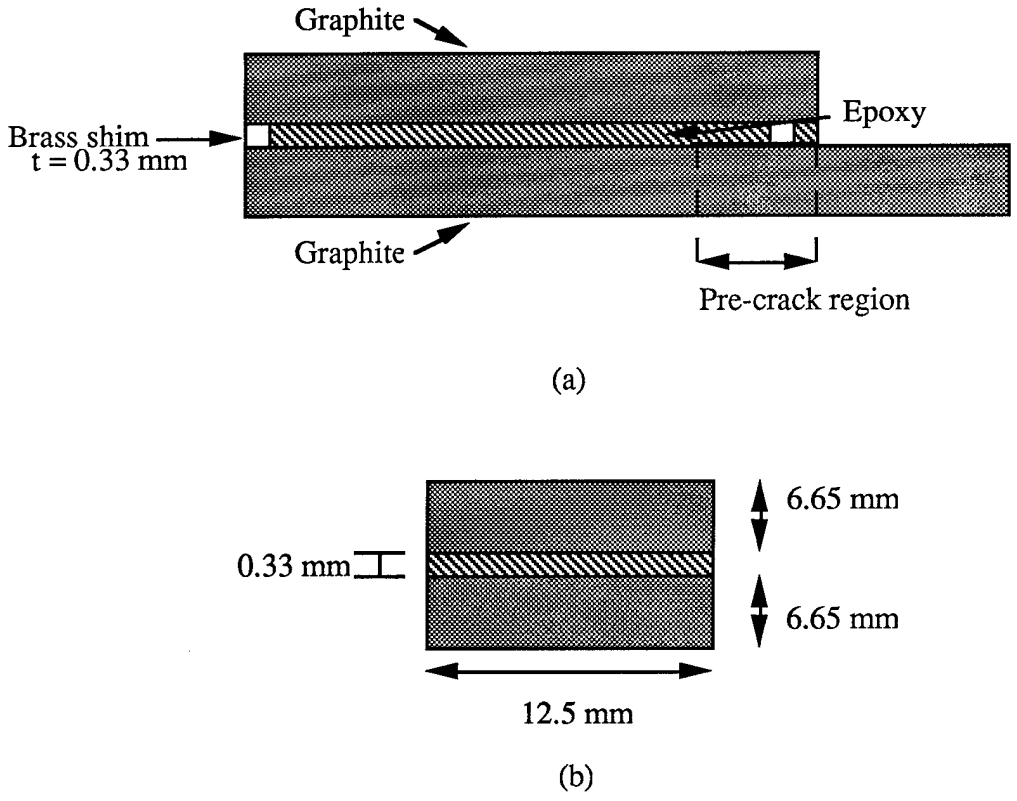

Figure 3.4: Flexural Peel specimen geometry: (a) Side view (b) Front view

This initial crack was grown to a length approximately equal to the length of the taped region in order to ensure that subsequent crack growth measurements would not

experience a "notch effect" from the pre-cracked region. After the initiation of this starter crack, the sample was loaded to desired load/cycle combinations to propagate the crack.

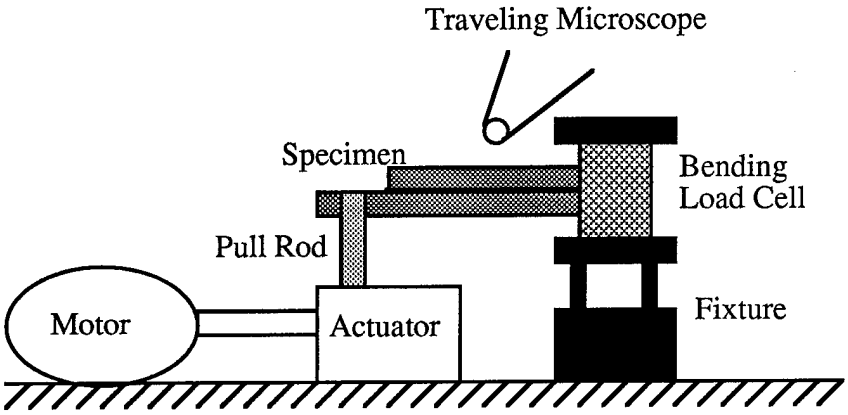

Figure 3.5: Schematic illustration of fatigue crack growth test apparatus[64]

Crack extension was observed by a traveling optical microscope at a magnification of 10 times. To aid the identification of the crack, a small amount of white correction fluid was applied to the side of the specimen. Fatigue crack growth rates were measured from approximately 10^{-3} to less than 10^{-7} mm/cycle. Fatigue threshold values were approached using a load-shedding procedure following the guideline of ASTM standard 647-88a.

Fatigue crack growth rates were correlated with the strain energy release rate, ΔG, determined from the fracture mechanics solution of the flexural peel specimens as

$$\Delta G = \frac{P^2(L+a)^2}{2E_o B}\left(\frac{1}{I} - \frac{1}{I^*}\right) + g \qquad [3.1]$$

where P is the maximum applied load for a fatigue cycle; E_o, the elastic modulus of the graphite substrate; B, the width of the specimen; L, the distance from the loading line to the pre-crack; and I and I^*, the moments of inertia of the lower beam and the composite beam respectively. Since the upper and lower graphite beams are of equal thickness for these experiments, I^* may be expressed as

$$I^* = I_o + I_i \frac{E_i}{E_o} \qquad [3.2]$$

where

$$I_i = \frac{Bh^3}{12} \qquad [3.3]$$

$$I_o = \frac{2B}{3}\left(t^3 + \frac{3ht^2}{2} + \frac{3h^2t}{4}\right) \qquad [3.4]$$

The residual term, g, in Equation [3.1] depends on the geometry and elastic properties of the two materials. For this case, however, the value of g turns out to be very small (less than 0.1 %) compared to the first term in Equation [3.1] and was therefore neglected in all subsequent calculations. A more comprehensive analysis of the analytical solution to the flexural peel geometry may be found elsewhere [65].

3.3.4 Finite Element Analysis

Numerical solutions were required in order to calculate the contributions to the total strain energy release rate from Mode I (tensile opening) and Mode II (in-plane shearing) crack tip fields. Therefore, finite element analysis was used to determine mixed mode parameters.

Following the method described by Zhang and Shang[65], G_I and G_{II} as well as the local phase angle

$$\phi = \tan^{-1} \frac{\tau_{xy}\left(\hat{r}\right)}{\sigma_{yy}\left(\hat{r}\right)} \qquad [3.5]$$

were calculated for the material combination and geometry specified in Sections 3.3.2 and 3.3.3. Figure 3.6a shows the finite element model used for these calculations. The mesh, created by PATRAN*, consisted of approximately 2000 isoparametric, 8-node elements.

* PATRAN is a trademark of PDA Engineering, Costa Mesa, MA.

Finer meshes were used near the interface and crack tip region, as seen in Figure 3.6b. Calculations were accomplished by ABAQUS# and yielded a G_{II}/G_I ratio of .5086 and a local phase angle of 38.0°.

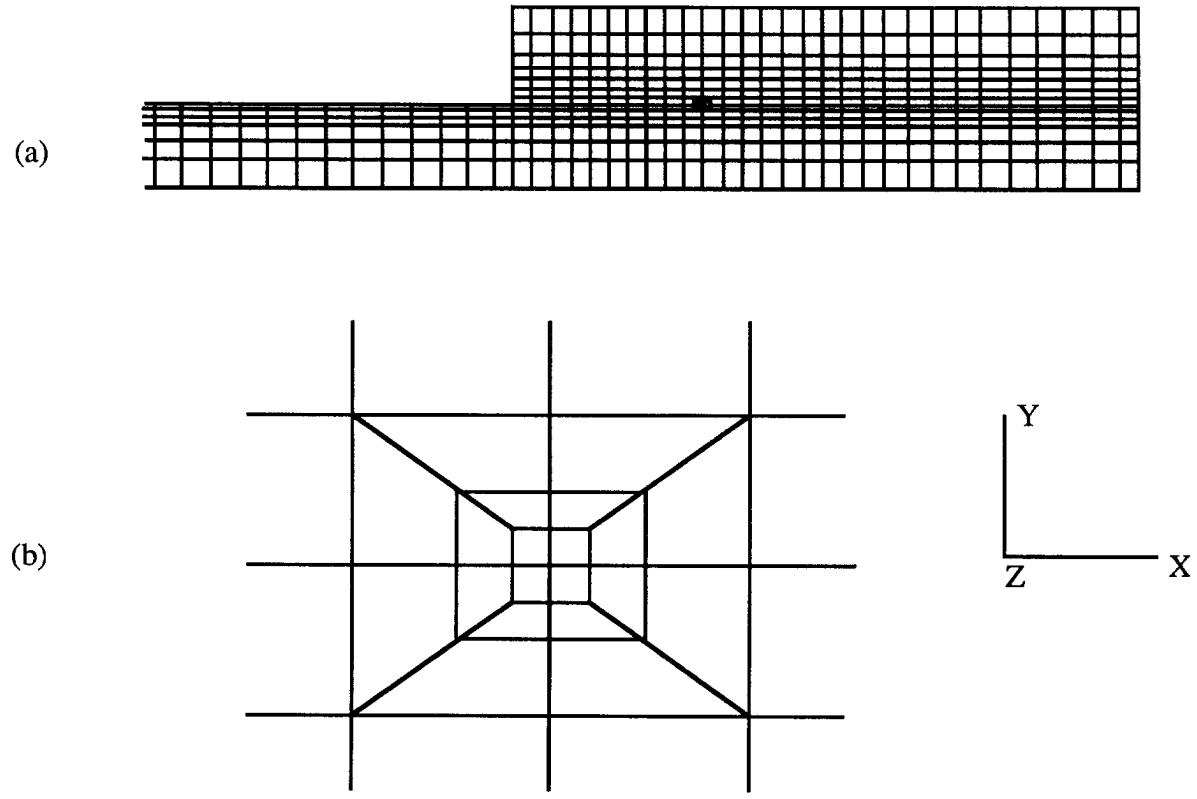

Figure 3.6: Finite element model of the flexural peel specimen: (a) mesh structure near the interface; (b) meshes near the crack tip

3.3.5 Crack Profile

Upon completion of the crack growth experiments, specimens were sectioned lengthwise using a diamond saw. One of the sectioned halves was polished down to 1mm diamond finish in order to provide a view of the crack profile. Polished specimens were viewed under both optical and scanning electron microscopes in order to characterize the crack path. Emphasis was placed on observing the crack path at regions of different strain

ABAQUS is a trademark of Hibbitt, Karlsson, and Sorenson, Providence, RI.

energy release rate (i.e. high, medium, and low) in order to determine if the crack tended to deviate from the interface with any recognizable pattern in any of these regimes.

3.4 Fracture Surface Analysis

Sectioned halves of specimens not used for crack profile analysis were broken open and used for fracture surface analysis. After sectioning and opening, specimens were first examined under optical microscope to determine if fracture was interfacial or cohesive. Samples were then coated with Au/Pd for a minimum of 180s and fracture surfaces were observed using SEM. The differences in fracture surfaces for specimens with different surface treatments and under the various strain energy release rate regimes were examined at the microscopic scale.

Chapter 4

Experimental Results

4.1 Effect of Oxygen Plasma Etching

As discussed in Chapter 2, current thought on graphite/epoxy adhesion is that the main contributions to adhesion come from surface roughness/interlocking effects, and chemical bonding effects. However, no general consensus exists as to the relative contributions of these effects. Further, the issue of how these contributions interplay when exposed to conditions of cyclic loading has received little attention to this point. Therefore, a set of experiments has been conducted to test the effects of an oxidative plasma on the adhesion of a graphite substrate and epoxy adhesive under conditions of cyclic loading.

4.1.1 Surface Characterization

With any adhesive bonding process, the surface chemistry and morphology of the substrate play a tremendous role in determining the overall strength of the interface. Recognizing this fact, a detailed study of the surfaces of the graphite specimens used was deemed a necessity. In order to fully characterize these surfaces and the effects of the etching process on them, a comprehensive examination of both the chemical and morphological changes from etching was performed before testing interfacial properties.

4.1.1.1 Surface Chemistry

X-ray photoelectron spectra were obtained for surfaces etched for 0, 5, 10, 15, and 30 minutes in an oxygen plasma. Wide scan spectra were taken for each sample but are not shown because they are all relatively similar showing a strong C1s peak and a weaker O1s

peak. A very weak N1s peak was seen on the untreated surface, but no N1s peak was observed for any of the other surfaces.

Narrow scan spectra of the C1s and the O1s peaks for the surfaces treated for 0, 15, and 30 minutes are shown in Figures 4.1 and 4.2 respectively. Quantitative analyses of the surfaces were obtained by measuring the area of the most intense peak for the particular element and applying the appropriate sensitivity factor. For each of the treatment times, the surface of the specimen was analyzed and mean concentrations of carbon and oxygen (expressed as atomic percentages) were determined. Table 4.1 summarizes the data obtained for the various graphite samples.

Table 4.1: Surface composition of PG for various treatment times

Treatment time	% Oxygen	% Carbon	O1s/C1s
0 minutes	18.62	81.38	0.229
5 minutes	23.81	76.19	0.313
10 minutes	22.80	77.20	0.295
15 minutes	24.33	75.67	0.322
30 minutes	22.91	77.09	0.297

In Figure 4.3, O1s/C1s ratios from the XPS narrow scan spectra for both the untreated and plasma treated specimens are shown. Note that the oxygen content on the surface rises quickly between the untreated surface and the surface treated for 5 minutes. Further treatment times resulted in no significant change in oxygen content out to the sample etched for 30 minutes. These results suggest that plasma treatment results in the addition of oxygen-containing functional groups to the edge surfaces, but that a saturation point is quickly reached. Similar results have been obtained for PG edge surfaces with different RF power and treatment pressures and out to longer treatment times[6], suggesting that the general observed behavior is a function of the graphite surface rather than one of specific operating parameters.

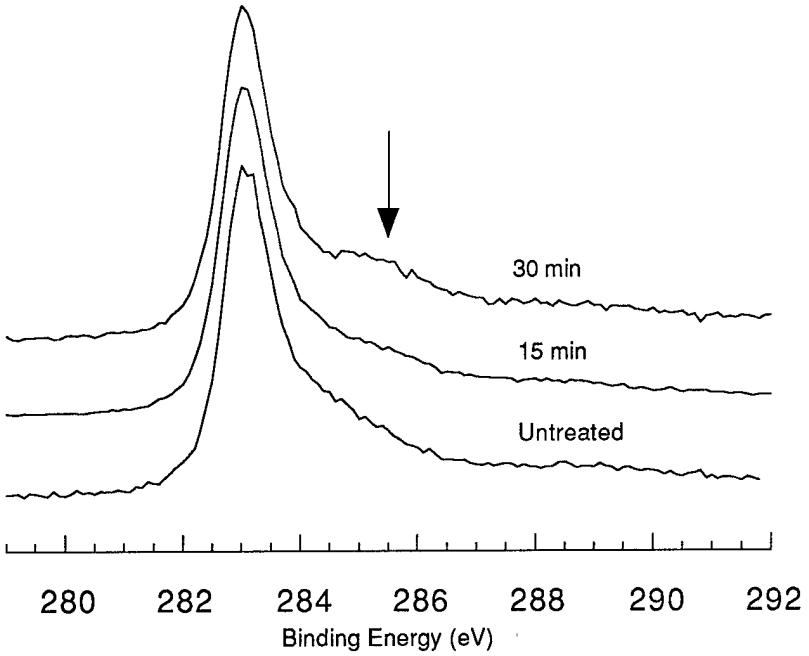

Figure 4.1: XPS narrow scan spectra for the C1s peak for various surface treatment times

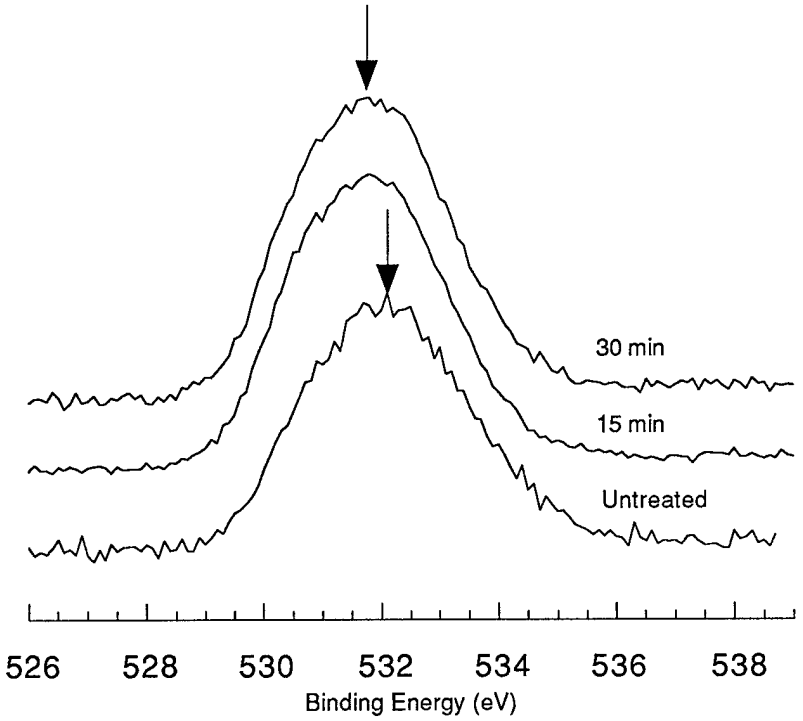

Figure 4.2: XPS narrow scan spectra for the O1s peak for various surface treatment times

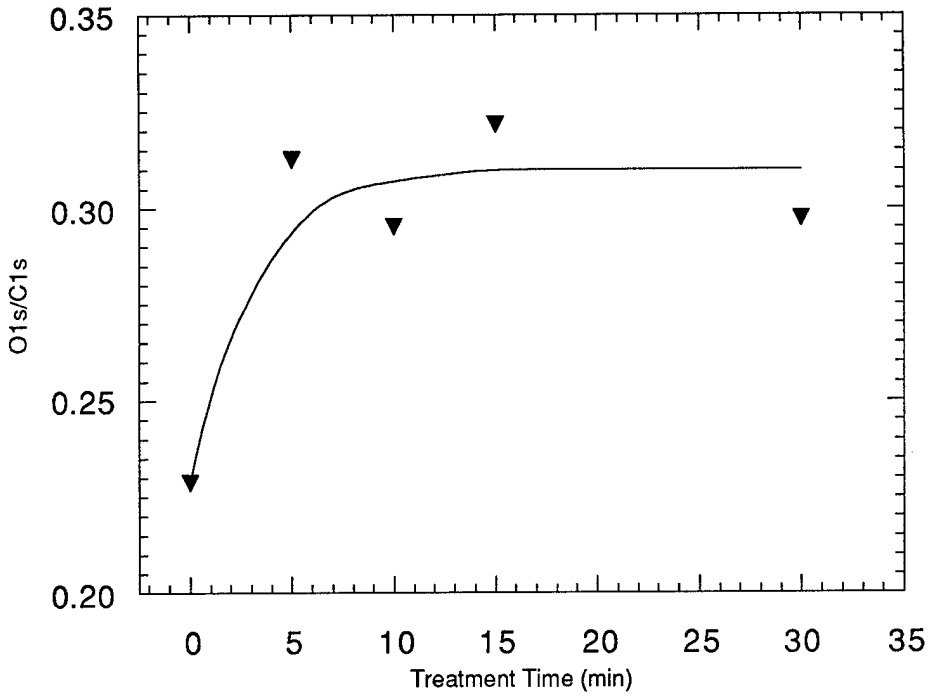

Figure 4.3: Effect of treatment time on the O1s/C1s ratio from XPS spectra

In addition to providing an assessment of the change in oxygen content caused by plasma treatment, narrow scan XPS spectra were also analyzed to give an indication of the type of bonding present on the graphite surface. Examination of the O1s peaks in Figure 4.2 reveals that the peaks for the etched surfaces are shifted slightly to the left (i.e. toward the lower binding energy component) in relation to that of the untreated surface. In the O1s spectrum, the lower energy component below about 532eV arises from =O type groups while the higher energy component arises from -O- type groups or CO, CO_2, O_2, and H_2O which may be present on the surface[27,66]. Evidence derived from the O1s spectra thus indicates that it is mainly =O groups which are added by plasma treatment.

Further clarification of the type of functional groups on the surface may be obtained by an analysis of the C1s peaks for the different surfaces. Visual inspection of these peaks shows an additional component present on the higher energy shoulder of the peaks for the

etched surfaces, as indicated in Figure 4.1. Computer analysis of these peaks was used to determine relative concentration of functional groups. The results of this analysis, shown in Table 4.2 below, indicate that the primary change in bonding caused by plasma treatment is the addition of >C=O groups to the surface. Similar changes in functionality have been noted for graphite surfaces etched both in O_2 [6,40] and CO_2[41] plasmas.

Table 4.2: Composition of the C1s peak for surfaces with various treatment times

Functional Groups	Peak Position	Etching time		
		Untreated	15 min	30 min
		(groups presented as % of total C1s peak)		
Primary C-C bond	283.0	48	43	43
C-OH; C-O-C	285.1	30	31	29
>C=O	287.1	15	19	20
π -->π^* transition (aromatic shake-up)	288.7	7	7	8

4.1.1.2 Surface Morphology

4.1.1.2.1 Surface Profilometry

The changes in morphology after the different surface treatment times were measured by surface profilometry in order to assess quantitative difference in roughness produced by the etching procedure. Results from profilometry did provide a quantitative measure of the general trend in surface roughness among the specimens. Computer analysis of surface profiles yielded the arithmetic average roughness (AA), or average deviation from the median. Calculated roughness values versus surface treatment time are displayed graphically in Figure 4.4 below. Note that although there is considerable uncertainty in the data, roughness values as well as the characteristic features of the respective profiles of the samples etched for 0, 15, and 30 minutes do provide differences worthy of discussion.

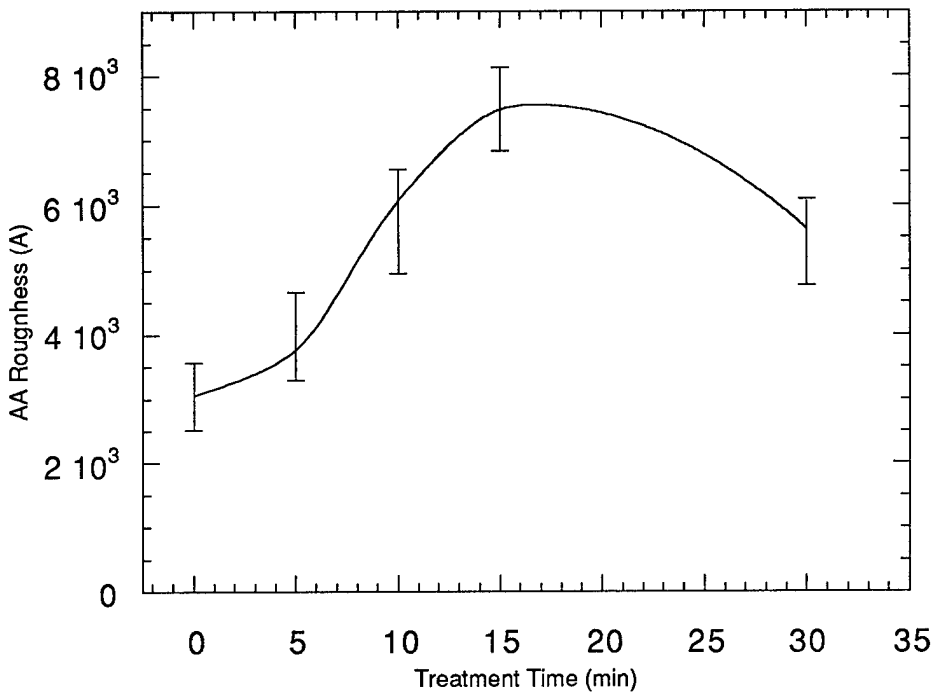

Figure 4.4: Arithmetic average roughness versus etching time

Scanning profiles of the untreated surface revealed the smoothest of the surfaces under study, as expected. However, the surface was far from atomically flat, and in fact it exhibited the characteristic morphological features shown in the typical profile of Fig 4.5. Of interest to note in this profile is that a characteristic peak/valley pattern with heights of approximately 10-15kÅ exists over a 50μm length scale. These peak/valley ranges are spaced approximately 10 to 15μm apart. Such spacing is consistent with what would be expected of any relatively soft surface polished as described earlier and may be attributed to the surface preparation process.

After a treatment time of 15 minutes, some clear roughening of the graphite is visible on the scanning profile as demonstrated in Figure 4.6. Of immediate note is that the peak/valley height has grown from 10 or 15kÅ to between 15 and 25kÅ over the same 50μm range. Furthermore, the characteristic length of these peaks remains on the 10 to

15μm scale. On the basis of this evidence alone it appears that the effect of the plasma etch was to preferentially attack irregularities in the surface produced by the polishing process, resulting in more pronounced surface features.

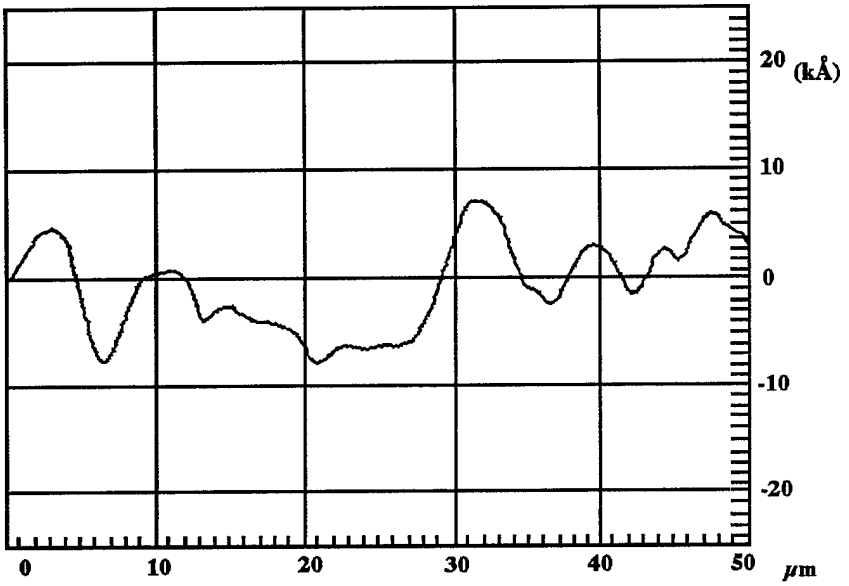

Figure 4.5: Typical profilometry scan for an untreated graphite specimen

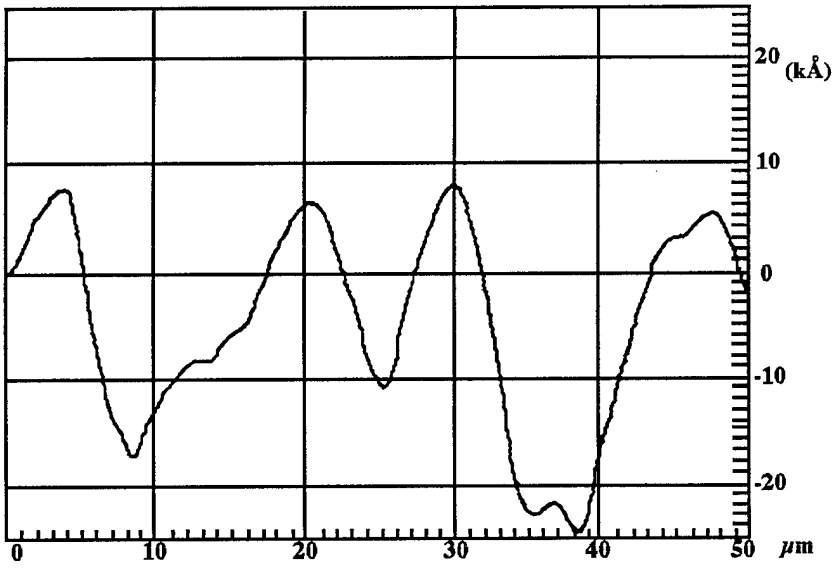

Figure 4.6: Typical profilometry scan for a sample etched for 15 minutes

Figure 4.7 is representative of the typical profile obtained for the graphite surfaces which had been etched 30 minutes. Roughness has decreased from the value obtained for the surface etched for 15 minutes but remains greater than that of the unetched specimen. The characteristic spacing of the peak/valley pattern remains, though the tops of the peaks and bottoms of the valleys appear more rounded than on samples etched for shorter periods of time. Such behavior suggests that an over-etched condition had been reached in which further etching of the valleys was being counterbalanced by an erosion of the tops of the peaks.

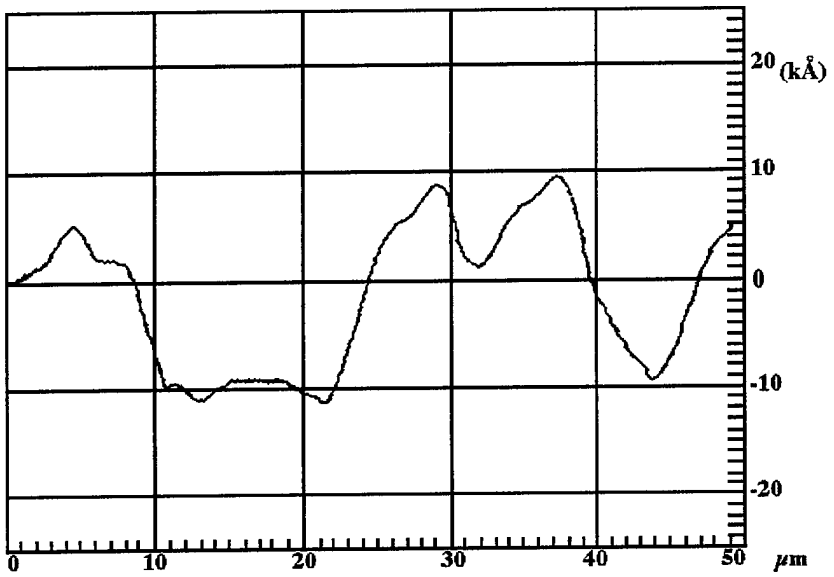

Figure 4.7: Typical profilometry scan for a sample etched for 30 minutes

Despite the varied results suggested by the surface profiles discussed above, caution must be taken not to reach wide ranging conclusions on the basis of these profiles alone. While the features mentioned above are noteworthy, profilometry is inherently limited by the fact that it provides only a two-dimensional picture of the surface. As a result, high-resolution microscopy is necessary in order to provide a clearer picture of the

surface and to supplement the results of profilometry in characterizing the morphological differences among samples with different treatment times.

4.1.1.2.2 SEM Observation

Further characterization of the different morphologies produced by the etching process was accomplished by viewing the samples under high resolution SEM. The SEM images of the top views of untreated, 15 minute, and 30 minute etched specimens help to identify more precisely the variations in morphology among the different treatment times, as shown in Fig. 4.8.

Upon initial inspection of the untreated sample, it is apparent that this surface is much smoother than either of the etched samples. The edge surfaces of successive basal planes are clearly visible and their regular stacking sequence gives a clear demonstration of the large amount of anisotropy present in the material. When viewed in this manner, the graphite surface has an appearance similar to that of a cross-section of layers of foil placed one on top of another. Aside from the presence of basal layers, other noteworthy morphological features of this surface appear to be the direct result of the polishing operation. One such feature present on the surface is a wave-like pattern running left to right across the surface. The successive "crests" running from top to bottom on the surface (Fig. 4.8a) are consistent with the direction of final polishing and may be attributed to the action of the abrasive across the surface. Closer examination of these edge surfaces reveal another result of the polishing process as some of these layers are bent in the direction of polishing (bottom to top on the photograph). The bending of some of the graphite planes can be more clearly seen under higher magnification as shown in Figure 4.9. This bending of the edges of the basal planes is important because it gives the

surface a smoother appearance. Whereas the stacking of layers perpendicular to the surface produces areas of micro-roughness between planes, bending of these planes

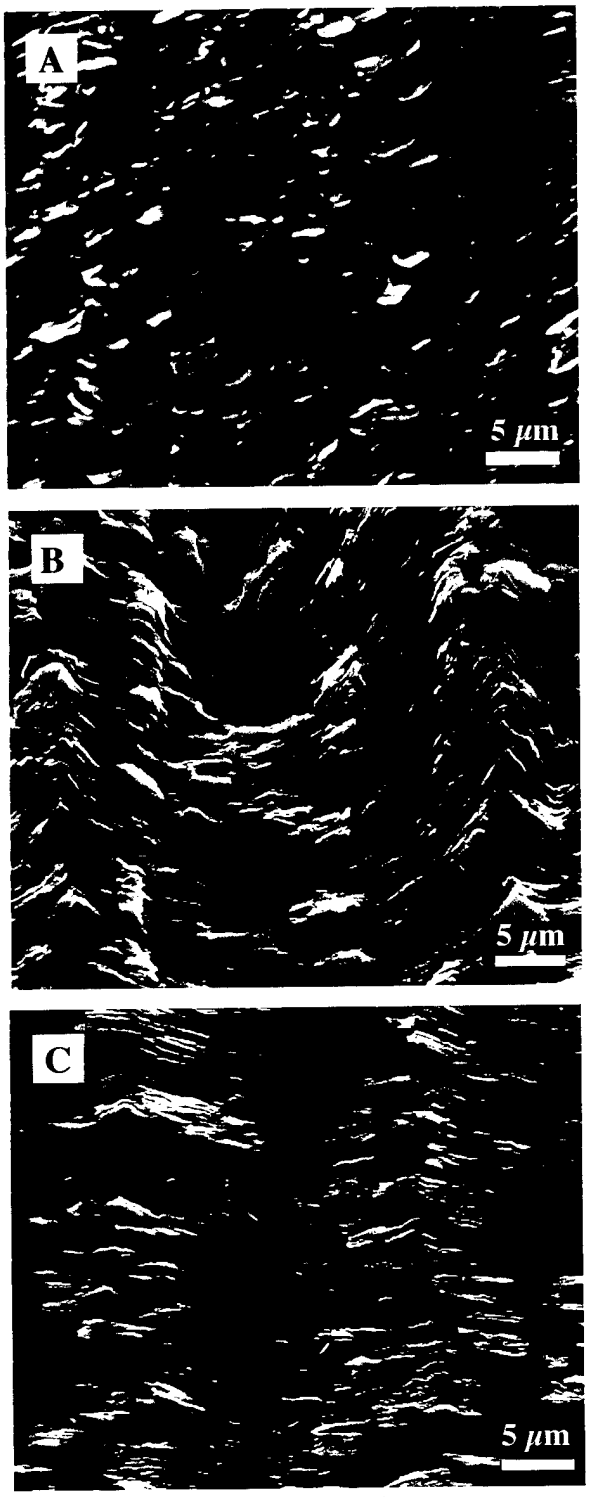

Figure 4.8: Top view of morphological changes caused by etching: (a) no etch; (b) 15 min etch; (c) 30 min etch

effectively removes such roughness. As a result, when an adhesive is applied to the surface, there are fewer areas for this adhesive to mechanically anchor itself to the surface. Furthermore, previous research[6] has demonstrated that the ability to add oxygen-containing functional groups is far less for basal surfaces as opposed to edge surfaces.

Other researchers have also noted a disruptive effect on the graphite surface from the polishing process. Nakahara and Sanada[7] used laser Raman spectroscopy to determine the ratio of edge carbon atoms to surface graphite basal planes. They attributed to the polishing process the production of a "disordered" layer which covers the inherent edge structure of the graphite. The concept of such a disordered layer is consistent with the observation of bent edge surfaces seen in Figure 4.9. This layer may also be likened to the weak, disordered outer layer often seen on the surface of untreated carbon fibers[67,68].

Figure 4.9: Higher magnification view of the untreated surface showing bent basal surfaces

In contrast to the untreated specimen, the surface of the sample etched for 15 minutes displays a marked degree of roughness. What appeared as a rather smooth, wave-like pattern on the untreated surface was transformed to much more of a peak and valley profile as a result of etching. Spacing of this pattern is relatively consistent on both samples, with high points on the morphology spaced approximately 20μm apart. However, peaks on the etched sample have a sharp, almost jagged, appearance compared to the gradual change in slope observed before the etching process took place. Under higher magnification, as in Figure 4.10, the sharpness of the peak areas of the surface is quite evident. This appearance supports the conclusion that the plasma attacked and amplified surface irregularities caused by the polishing process.

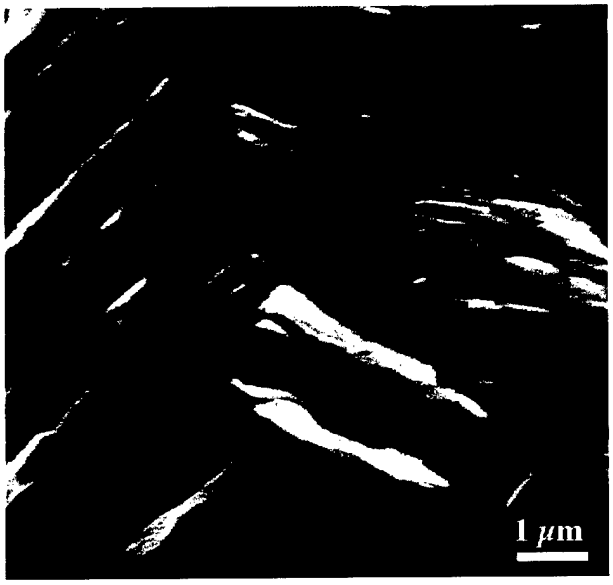

Figure 4.10: Higher magnification view of 15 minute etched surface illustrating the sharp peak-like features on the surface

Comparing the untreated and etched morphologies of Figures 4.9 and 4.10, the result of etching of the bent basal surfaces can also be seen. Note in Figure 4.10 that the spacing between basal planes is much more visible than in Figure 4.9 for the unetched

surface. What is being observed is the effect of etching away the basal surfaces, or the disordered layer. The resulting surface is much more accessible to penetration by an adhesive and presents far more opportunities for mechanical interlocking to occur.

The effects of over-etching are seen on the surface of the sample exposed to the oxygen plasma for 30 minutes. While the characteristic repeating pattern on the order of 20μm is still present on this sample, it is not nearly as well defined as it was on the 15 minute sample. Confirming the suspicions aroused by profilometry, the sharpness of the peaks which defined the 15 minute sample are no longer present. The morphology is best described as one of "rolling hills" distinct from the wave pattern of the untreated sample and the peak and valley pattern of the sample etched for 15 minutes. These observations lead to the conclusion that an equilibrium condition was reached in which further etching into the sample came at the cost of eroding away the tops of the peaks.

4.1.2 Crack Growth

Measured fatigue crack growth rates were correlated with strain energy release rate, ΔG, for the three surface treatment times of 0, 15, and 30 minutes as shown in Fig. 4.11. For the case of the plasma treated specimens, the crack growth curves consisted of a power law regime, in which the log da/dN-log ΔG plot is linear, and a near threshold regime, where the fatigue crack growth rate decreases asymptotically on the log da/dN-log ΔG plot. For the case of the untreated surface, the fatigue crack growth curve is almost entirely in the linear regime, with a slight downturn observed only below a da/dN of 10^{-7}mm/cycle. The power law exponent, n, and the power law coefficient, A, obtained by a least squared fit of the linear regimes of each sample are shown in Table 4.2.

For each of the surface conditions studied, the samples displayed a strong sensitivity to the strain energy release rate, as is evidenced by the high slopes of each of the

fatigue crack growth curves. Though the sensitivity of crack growth rate to ΔG is much less for the etched surfaces, even the lowest slope, 5.2, obtained for the surface etched for 30 minutes, is quite steep for an engineering material. Slopes of this magnitude indicate that even small changes in loading conditions could be enough to cause catastrophic failure. This sensitivity to loading represents an engineering design problem for finite life calculations since even minor design alterations or small analysis errors could cause large changes in calculated results. As an alternative, infinite life design approaches may be used. To this end, the concept of crack growth threshold, defined as the strain energy release rate at which da/dN falls below 10^{-7}mm/cycle, becomes important.

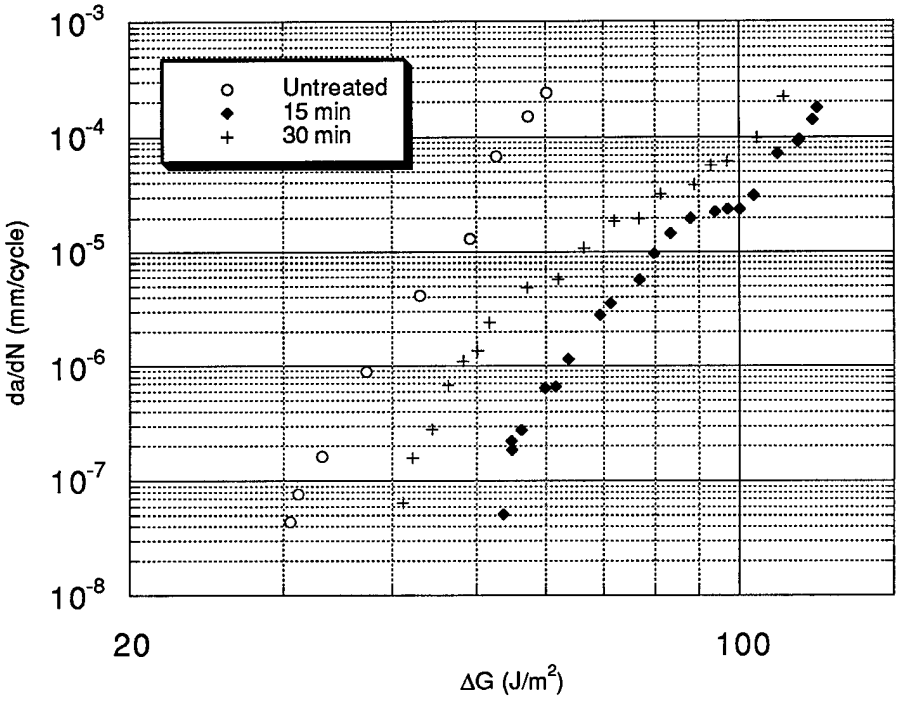

Figure 4.11: Fatigue crack growth curves for specimens with surfaces etched for various times

Table 4.3: Power law coefficients and exponents of FP specimens with different surface treatment times

Treatment time	n	A
0 minutes	12.5	1.72×10^{-26}
15 minutes	7.1	2.38×10^{-20}
30 minutes	5.2	5.40×10^{-17}

By using ΔG_{th} to evaluate improvements in adhesion with surface treatment, it is seen that the 15 minute plasma etch almost doubles the interfacial strength over that of the untreated specimen. After this treatment time, ΔG_{th} increases from a value of $30 J/m^2$ to $54 J/m^2$. However, with an additional 15 minutes of etching time, the threshold strength decreases to $41 J/m^2$, a clear sign of the effects of over-etching discussed previously.

One final point of interest is that the fatigue crack growth curves for the two etched samples begin to converge as strain energy release rate increases. While the separation between all three curves in the near threshold regime is significant, it is only the unetched specimen which continues its divergence from the other two curves at higher ΔG values. This divergence seen in the unetched specimen is the result of a large increase in fatigue crack growth resistance for the treated specimens along the entire curve. The convergence of the treated specimens at higher strain energy release rates would seem to suggest that a common failure mechanism is at work, particularly at higher loads, and that this mechanism is not seen in the untreated sample. Analysis of fracture surfaces of all the samples was required to confirm these suspicions and define the precise failure mechanisms at work.

4.1.3 Failure Mechanisms

Upon completion of the fatigue crack growth tests, specimens were sectioned and broken open to reveal the fracture surfaces. Samples were first inspected visually as well

as under optical microscope, but neither of these methods proved adequate to characterize the surfaces. Therefore, scanning electron microscopy was utilized to characterize the various failure mechanisms and fracture morphologies of the specimens. Pictures taken from SEM clearly revealed that different failure modes existed between the treated and untreated specimens. Along the entire fracture surface of the untreated specimens, failure was interfacial, as seen in Figure 4.12. On the lower graphite surface, edge surfaces of basal planes are exposed, and a mirror image imprint of this graphite morphology can be seen along the upper (epoxy) surface. This failure pattern indicated that the crack was following a path along the lower graphite surface and that the epoxy adhesive was being pulled from this surface as the crack propagated (left to right across the photographs, as indicated). Higher magnification photographs of this pattern, as in Figure 4.13, further clarify the nature of failure as predominantly Mode I opening of the crack surfaces perpendicular to the direction of propagation.

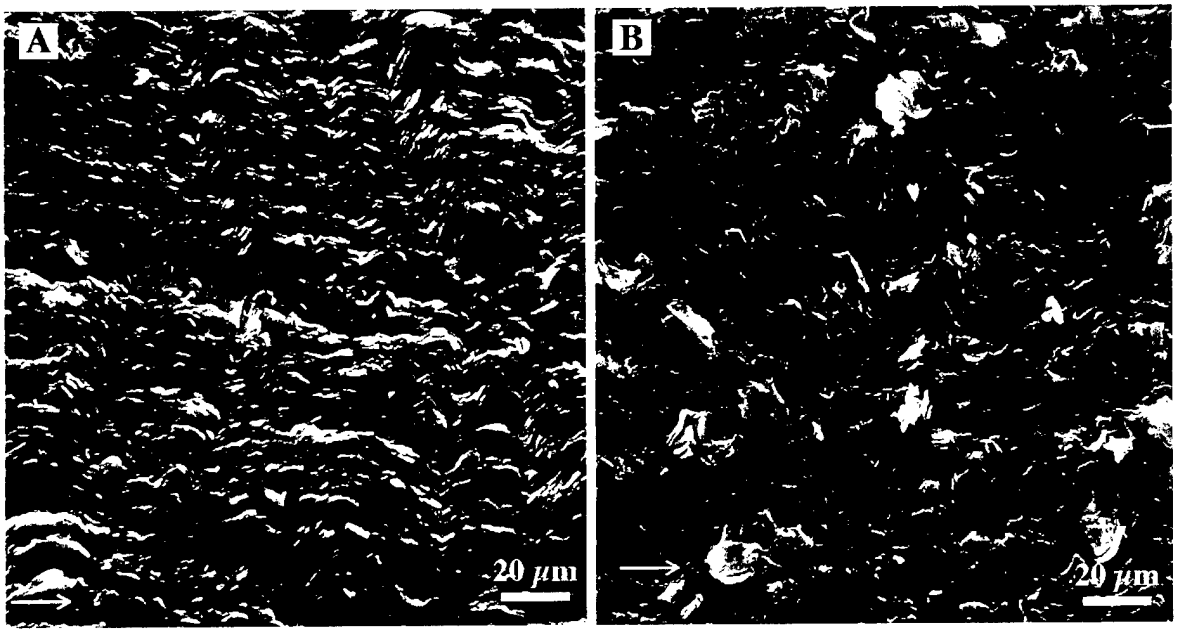

Figure 4.12: Fracture surfaces of an untreated specimen: (a) graphite side; (b) polymer side

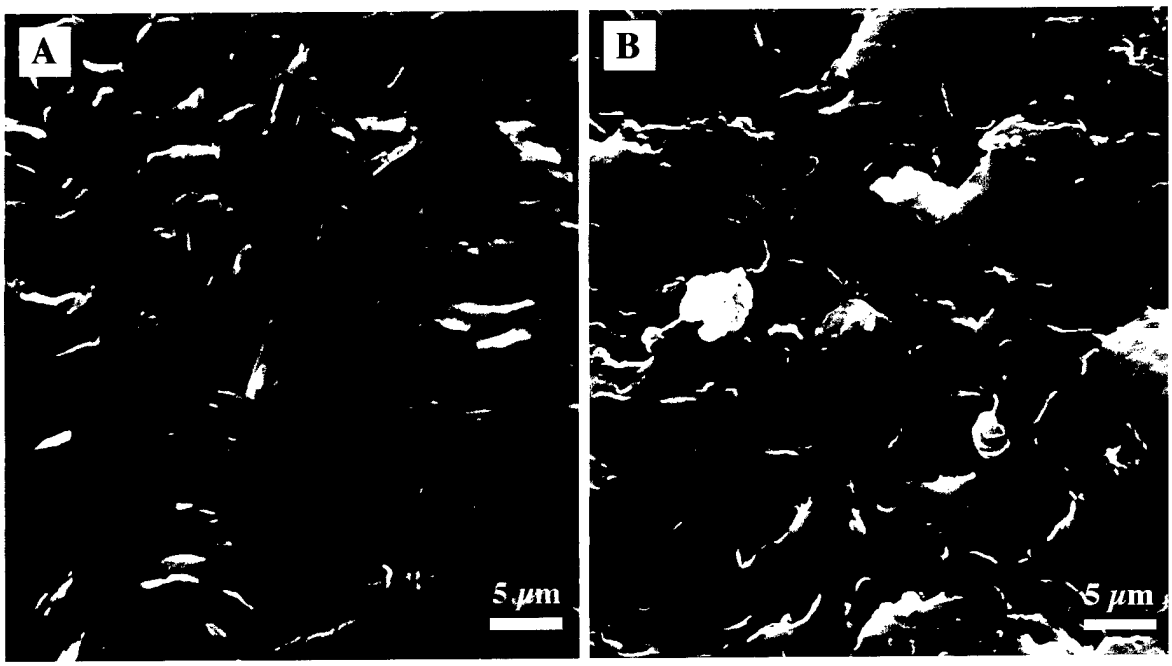

Figure 4.13: Higher magnification view of the fracture surfaces of an untreated specimen: (a) graphite side; (b) polymer side

Examination of the fracture surfaces for the sample etched for 15 minutes showed that in sharp contrast to the interfacial failure seen on the untreated surfaces, the failure mode had now become one of almost entirely cohesive failure. Figure 4.14 shows the bottom graphite surface of a FP specimen which had been etched for 15 minutes, as well as a higher magnification view of both top and bottom fracture surfaces. These surfaces were covered by a layer of epoxy having a shingle-like pattern with facets running parallel to the crack front. Similar morphology has been seen on cohesive failure surfaces in other adhesively bonded systems when crack growth occurred under predominantly shear (Mode II) conditions[69]. As threshold ΔG values were approached, the samples exhibited a slightly mixed failure mode, as seen on the bottom graphite fracture surface shown in

Figure 4.15. On this surface, some edge surfaces are visible, like those seen on the untreated surface. However, the majority of the surface is still covered with the shingle pattern of the epoxy indicating mostly cohesive failure.

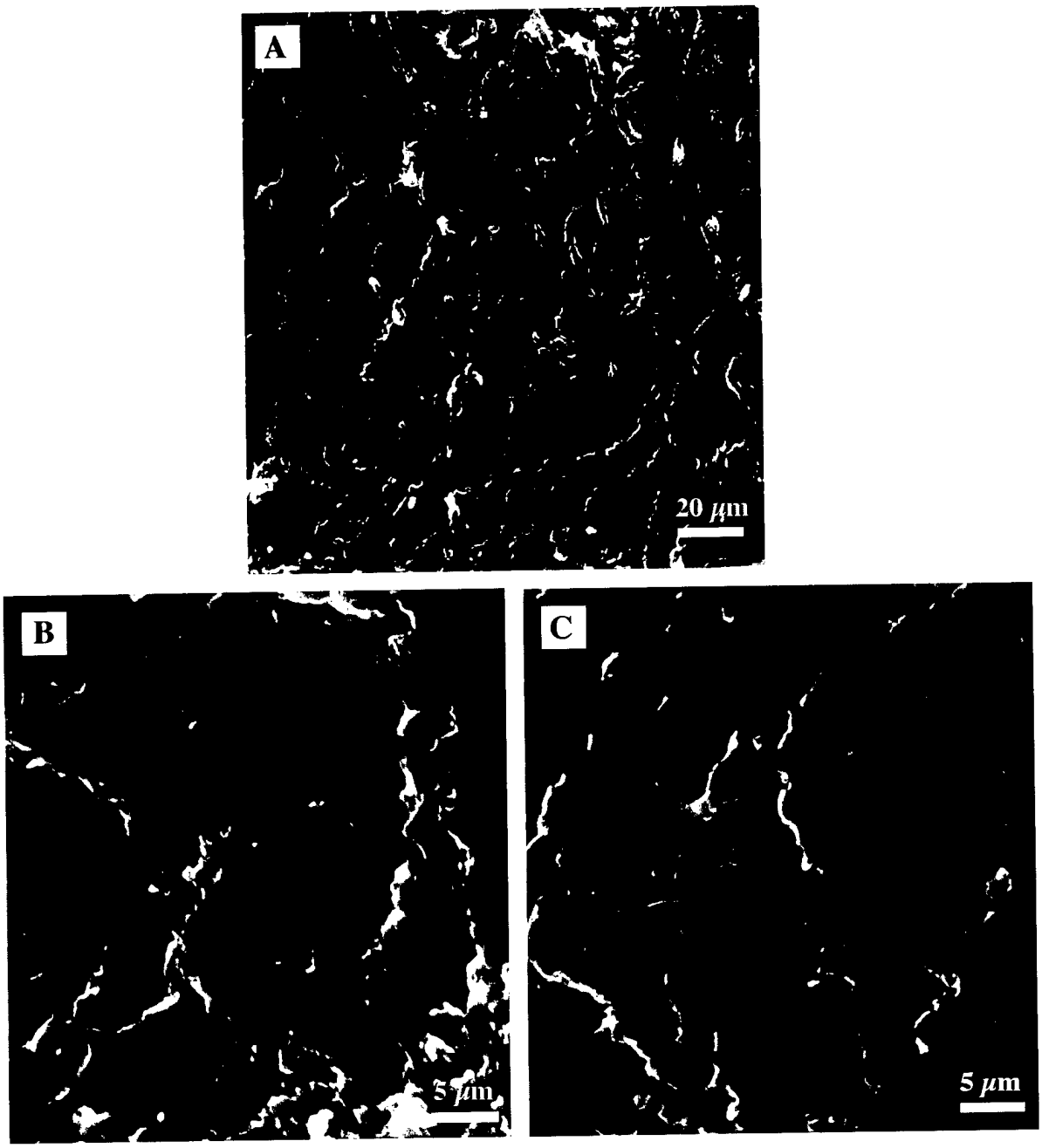

Figure 4.14: Fracture surfaces of a FP specimen with 15 minute treatment time: (a) graphite side x500; (b) graphite side x2000; (c) polymer side x2000

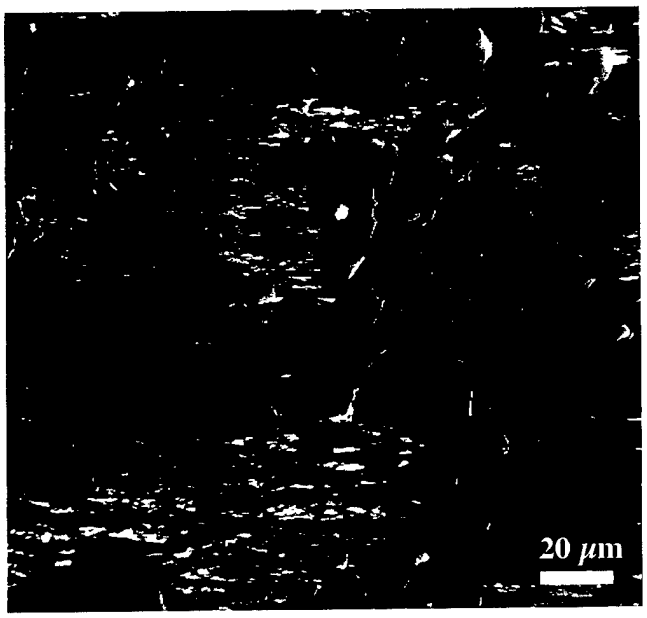

Figure 4.15: Near-threshold fracture surface (bottom) of FP specimen with 15 minute treatment time

When treatment time was increased to 30 minutes, the fracture pattern took on a much larger mixed character than was seen on the 15 minute etched surfaces. A representative picture of the bottom fracture surface, such as Figure 4.16, has almost a 50/50 mix of exposed edge surfaces and polymer "shingles". Higher magnification pictures of both of these areas (Fig. 4.17) distinctly show the mixed nature of the failure. Figure 4.17a-b reveal the mirror images of an area of interfacial failure. Note that these images are almost identical to the pattern seen in Figure 4.13 for the unetched surface. Figure 4.17c-d, on the other hand, are marked by the polymer facets like those seen covering the surface of the sample etched for 15 minutes (Fig. 4.14).

Figure 4.16: Bottom fracture surface of FP specimen with 30 minute treatment time

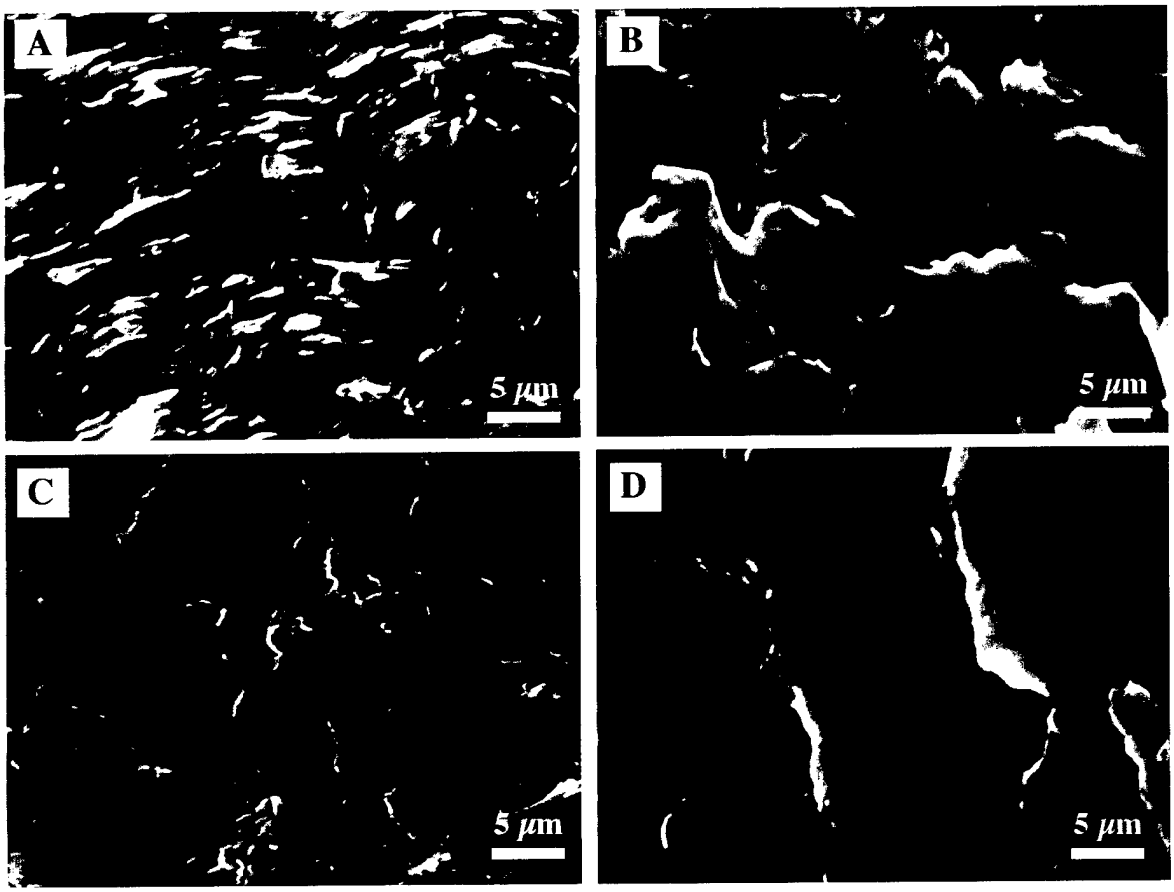

Figure 4.17: Mixed nature of failure seen on FP specimen with 30 minute treatment time: (a) interfacial bottom; (b) interfacial top; (c) cohesive bottom; (d) cohesive top

4.2 Effect of Post-Etching Heat Treatment

4.2.1 Surface Characterization

The main objective of the heat treatment process was to remove the chemical effects (i.e. added oxygen-containing functional groups) caused by the etching process while maintaining the morphological effects (i.e. surface roughening). Therefore, surface characterization was conducted using the same methods described in Section 4.1.1 in order to allow for direct comparison between the unetched, etched, and etched and heat treated surfaces.

4.2.1.1 Surface Chemistry

X-ray photoelectron spectra were obtained for surfaces heat treated after etching for 15 and 30 minutes. Wide scan spectra once again showed a strong C1s peak and a somewhat weaker O1s peak for both surfaces. Nitrogen was not present on either surface. Narrow scan spectra of the C1s and O1s peaks were also obtained for these heat treated surfaces and are shown in Figures 4.18 and 4.19 respectively along with the same peaks on the unetched surface for comparison. By analyzing these peaks, the relative concentrations of carbon and oxygen on each surface were determined. The results of this analysis, which are presented in Table 4.3 below, demonstrate that the heat treatment was successful in reducing the surface oxygen content back to the level of the unetched specimen. The O1s/C1s ratios for the unetched and 15HT (heat treated after an etching time of 15 minutes) are nearly identical, with the ratio for the 30HT specimen only slightly lower.

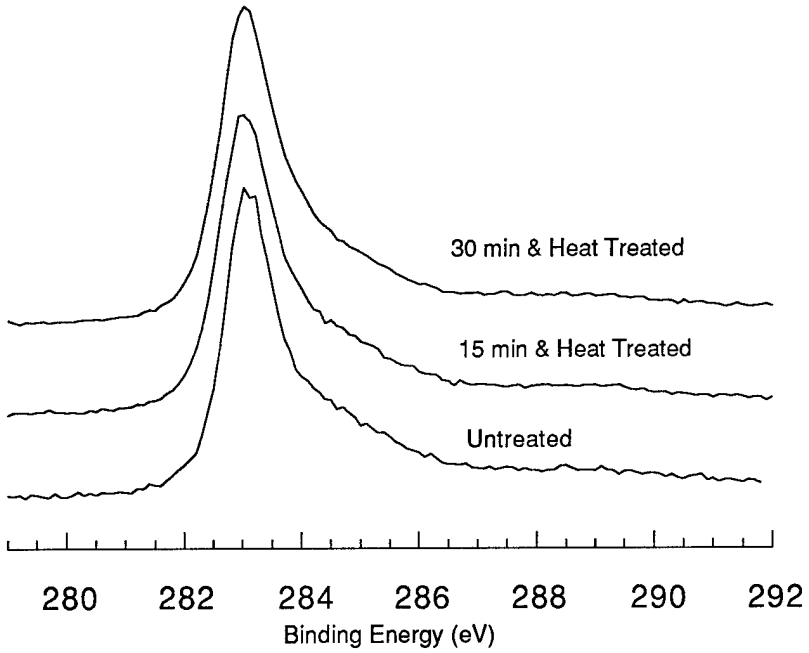

Figure 4.18: XPS narrow scan spectra for the C1s peak for various surface treatments

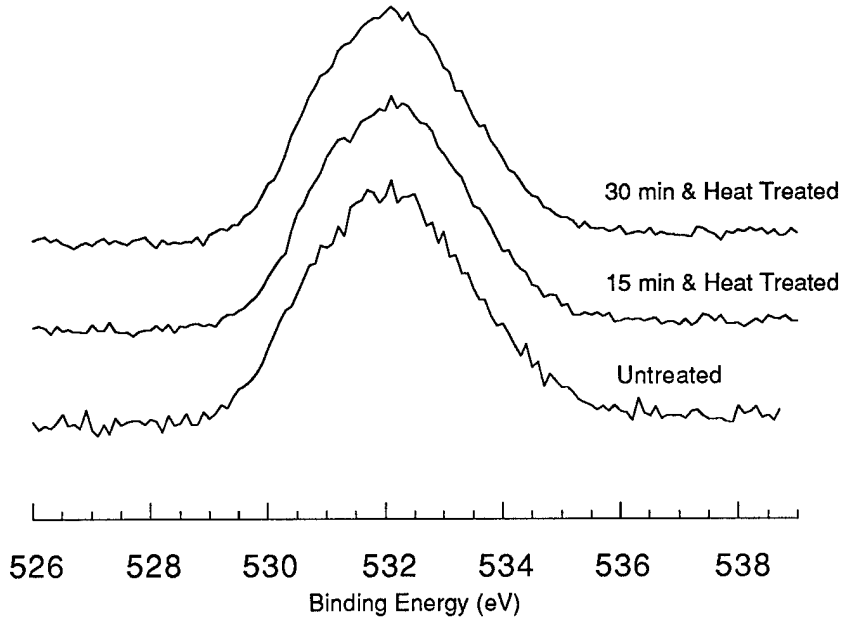

Figure 4.19: XPS narrow scan spectra for the O1s peak for various surface treatments

Table 4.4: Surface composition of PG for various treatments

Treatment	% Oxygen	% Carbon	O1s/C1s
no treatment	18.62	81.38	0.229
15 HT	19.13	80.87	0.236
30 HT	17.18	82.82	0.207

Comparison of the narrow scan carbon and oxygen peak locations and shapes for the three surfaces mentioned above give an indication of the type of oxygen-containing functional groups present. It is not possible, by visual inspection alone, to discern any significant difference between either the O1s or C1s peaks of different surface conditions. Recall that a noticeable difference was present on both peaks as a result of >C=O groups on the etched surfaces. The fact that after heat treatment, such differences are no longer present gives an indication that these additional =O functional groups are no longer present. Computer analysis of the C1s peaks for the heat treated surfaces confirms this conclusion, as shown in Table 4.5 below. Note that the concentration of double-bonded oxygen-containing functional groups has been reduced to pre-etching levels. The removal of >C=O groups, coupled with the reduction in overall oxygen content lead to the conclusion that, from the chemical perspective, the goals of heat treatment were achieved.

Table 4.5: Composition of the C1s peak for surfaces with various treatments

Functional Groups	Peak Position	Surface Treatment		
		Untreated	15HT	30HT
		(groups presented as % of total C1s peak)		
Primary C-C bond	283.0	48	46	47
C-OH; C-O-C	285.1	30	30	31
>C=O	287.1	15	16	15
π --> π^* transition (aromatic shake-up)	288.7	7	8	7

4.2.1.2 Surface Morphology

4.2.1.2.1 Surface Profilometry

In order to determine if heat treatment had resulted in any reconstruction of the graphite surface, profilometry was once again utilized for heat treated specimens. Computer-determined values of AA roughness demonstrated that a significant difference in roughness existed between the 15HT and 30HT specimens. Average roughness seen on the 15HT specimen was 7266Å and on the 30HT specimen was 5150Å. These values are slightly less than the average roughness calculated for the surfaces which had been etched only. However, the uncertainty for both the etched and etched and heat treated surfaces was on the order of approximately 1500Å. Therefore, it is not possible to differentiate between the etched and etched and heat treated surfaces using profilometry. This fact is demonstrated graphically in Figure 4.20. Surface profiles for the heat treated samples also were inadequate for the purpose of differentiating between those surfaces which had been heat treated and those which had not. Profiles once again indicated that a somewhat regular pattern existed on the surface with spacing of 10 to 20μm as seen in Figs. 4.5 through 4.7.

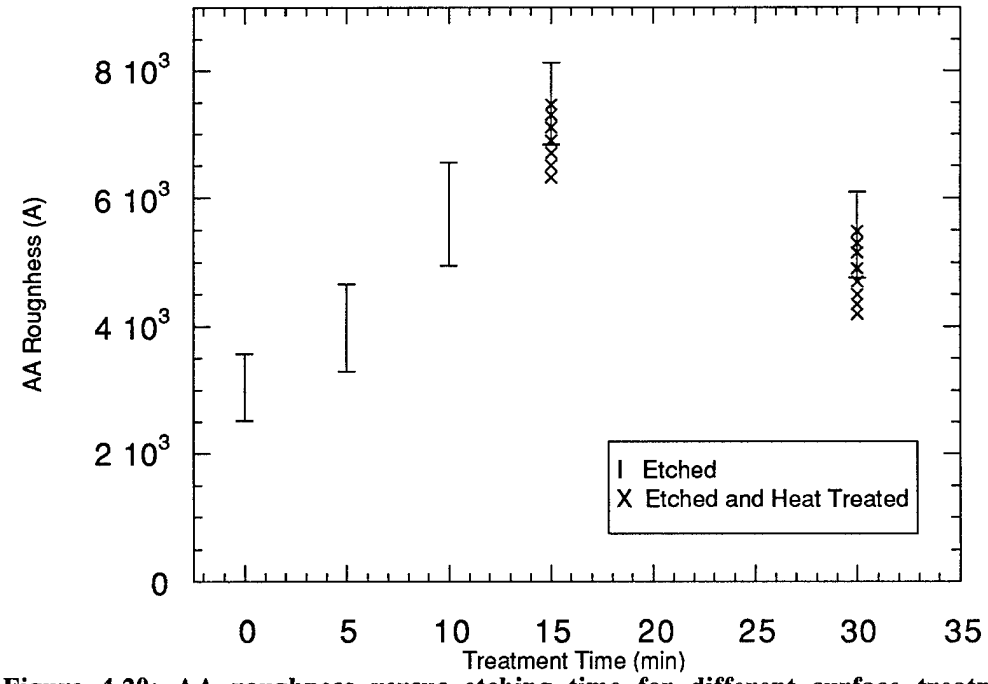

Figure 4.20: AA roughness versus etching time for different surface treatments

4.2.1.2.2 SEM Observation

Surface profiles and roughness calculations indicated that the basic surface morphology of the graphite was unchanged by heat treatment. High resolution SEM was used to verify these findings. Examination of the 15HT surface revealed the same surface features as were present on the 15 minute etched-only surface. Direct comparison between these two surfaces yields little substantive difference, as seen in Figure 4.21. Well defined rows of sharp peaks spaced on the order of 15mm dominate the surface. The spacing and orientation of these peaks are consistent with direction of polishing, supporting the conclusion that plasma etching preferentially attacks irregularities in the surface present as a result of the polishing process.

Figure 4.21: Surface morphology of surfaces etched for 15 minutes: (a) etched only; (b) etched and heat treated

In Figure 4.22, the 30 minute etched-only and the 30HT surfaces are shown side by side for comparison. As was the case for the shorter etching time, the general surface morphology of the two samples is the same. Both surfaces retain the roughness pattern visible on the surfaces etched for only 15 minutes. However, the sharpness of the peaks is

no longer as evident. Rather, rounded tops are present where the peaks once existed, possibly because of over-etching.

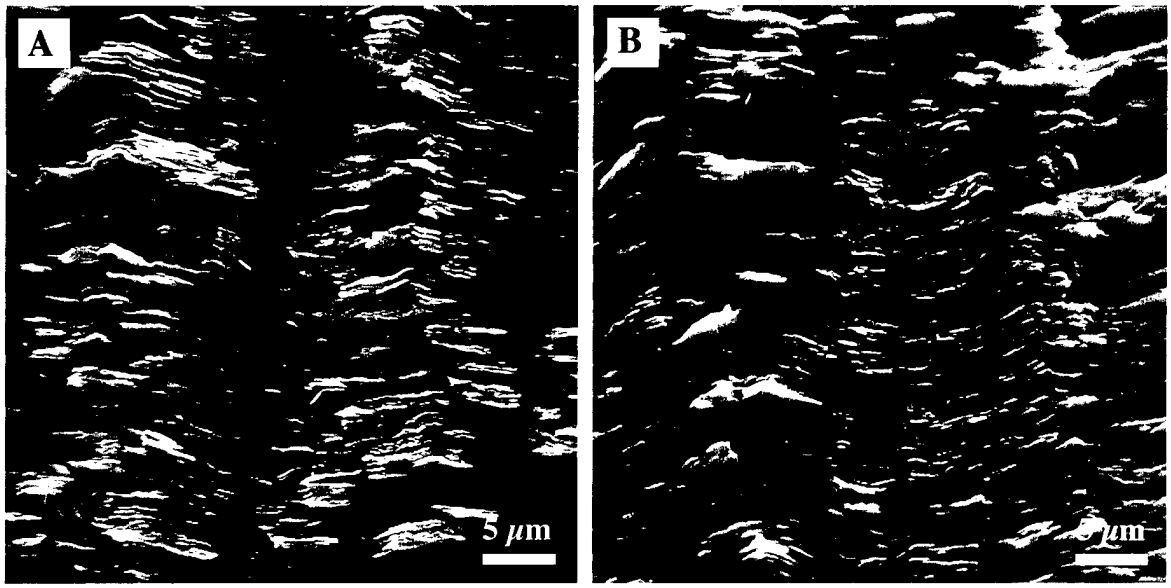

Figure 4.22: Surface morphology of surfaces etched for 30 minutes: (a) etched only; (b) etched and heat treated

4.2.2. Crack Growth

Heat treated specimens etched previously for 15 and 30 minutes were tested using the flexural peel geometry to investigate the effects of heat treatment on fatigue crack growth. Crack growth rates were determined in the same manner as described for the etched samples, and the strain energy release rates were calculated using Equation [3.1]. Since surface characterization had identified the loss of surface functionality in the form of =O type groups as the primary result of heat treatment, any changes in crack growth behavior could then be attributed to the decrease in chemical bonding across the graphite/epoxy interface.

Crack growth curves for the 15 minute etched-only as well as for the 15HT condition are shown in Figure 4.21 along with the reference curve for the untreated surface condition. Like the specimens with the etched-only condition, the curve for the 15HT

condition has considerably more resistance to crack growth than do specimens made from samples with untreated surfaces. At crack high growth rates, particularly as ΔG critical is approached, the curves for the two treated surface conditions run very close together. As threshold ΔG values are approached, however, the difference between the two curves becomes more distinct. At threshold, the ΔG_{th} for the 15HT curve is $47 J/m^2$ compared with a value of $54 J/m^2$ for the 15 minute etched-only condition, a 13% loss in total threshold strength as a result of heat treatment. Considering that the specimen-to-specimen variation in ΔG_{th} for the same surface condition was approximately 5%, differences seen in Figure 4.23 may be attributed to a slight loss of interfacial strength rather than simply experimental scatter.

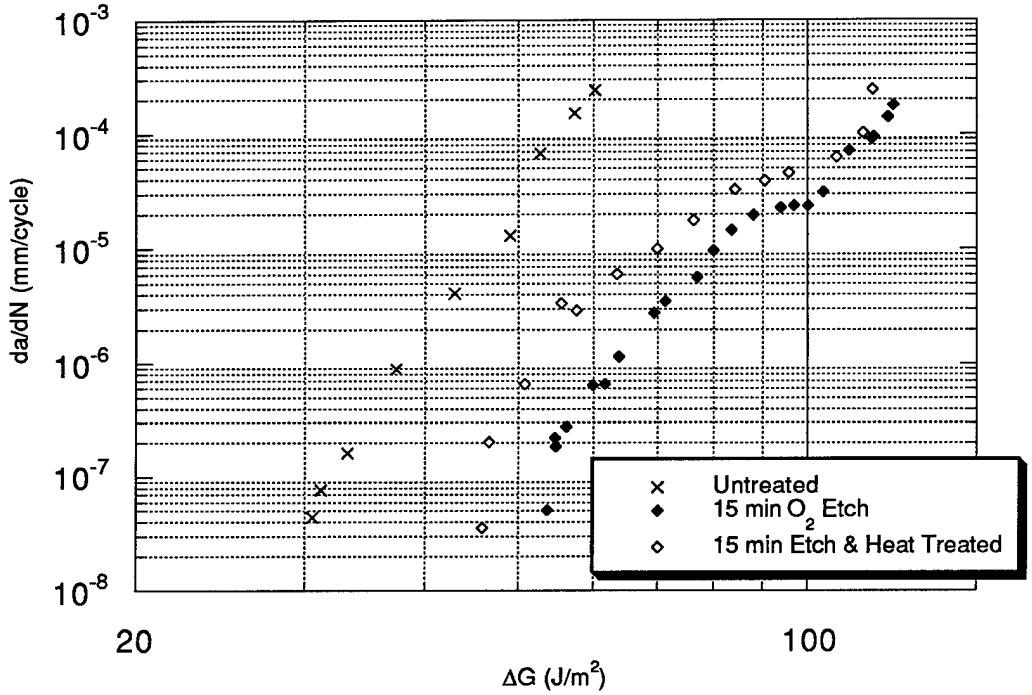

Figure 4.23: Fatigue crack growth curves for 15 minute etched-only and 15HT specimens

The difference in crack growth curves between the 30 minute etched-only and 30HT specimens is less than for the 15 minute conditions described above. In Figure 4.22, curves for both the etched and etched and heat treated conditions are plotted along

side the untreated reference curve. Once again, both treated surfaces have much greater fatigue crack growth resistance than the untreated specimens. Curves for the treated surfaces are intertwined for nearly the entire spectrum of crack growth rates. Only very near to threshold crack growth rates is a small divergence seen between the 30 minute etched-only and 30HT curves, and even here the difference ($38J/m^2$ as opposed to $41J/m^2$) is only approximately 7%. Recalling that the specimen-to-specimen scatter in these fatigue tests was approximately 5%, the chemical effect, though it may be present, becomes very difficult to assign. In this case, any weakening of the interface due to loss of bonding across the interface, is at best minimal and almost impossible to differentiate from experimental scatter.

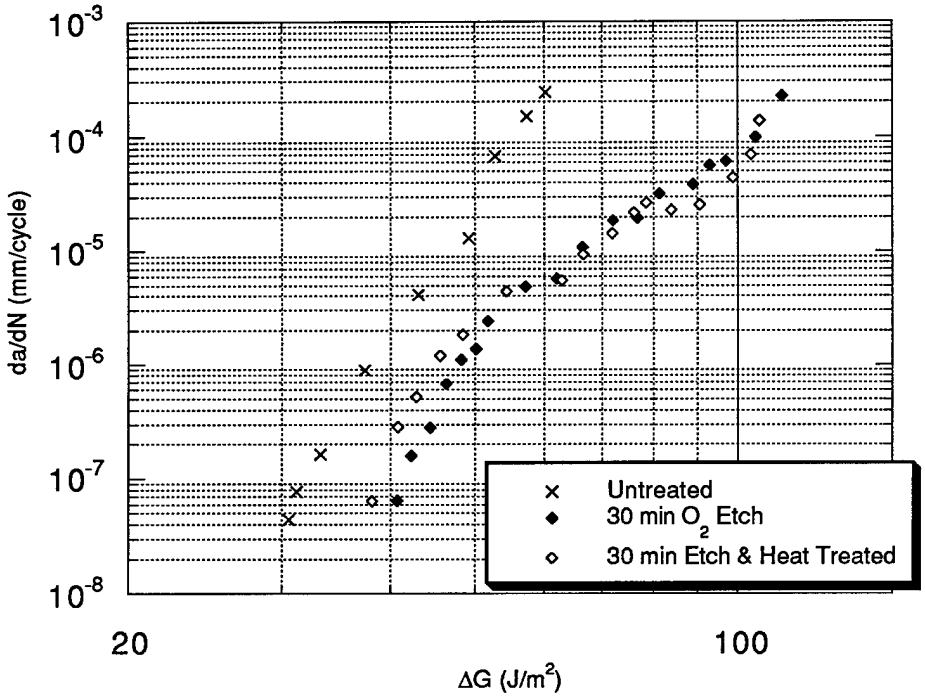

Figure 4.24: Fatigue crack growth curves for 30 minute etched-only and 30HT specimens

4.2.3 Failure Mechanisms

The fracture surfaces of heat treated specimens were characterized by scanning electron microscopy. Failure modes seen under SEM examination were consistent with

crack growth data, which showed that the graphite/epoxy interface for both surfaces was stronger than the untreated surface but weaker than their etched-only counterparts. For both the 15HT and the 30HT specimens, fracture surfaces were characterized by a mix of interfacial and cohesive failure. Differences in failure mechanism between the two surface conditions varied in degree rather than by type. Photographs of the bottom fracture surfaces of these two conditions are shown in Figure 4.25 to give the general trend for the mixed fracture pattern visible on the surfaces. Under higher magnification, as in Figure 4.26, it is clear that the regions of cohesive and interfacial failure are consistent with those seen on the etched-only fracture surfaces.

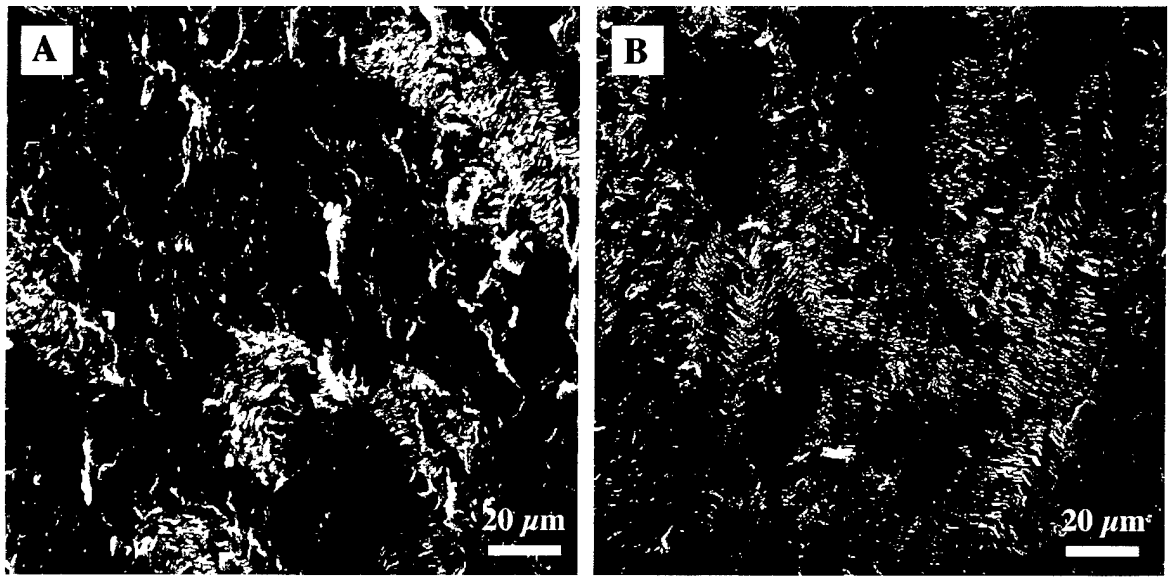

Figure 4.25: Bottom fracture surfaces of heat treated specimens: (a) 15HT; (b) 30HT

Low magnification photographs of the fracture surfaces of the five surface conditions studied in these series of experiments are shown in Figure 4.27(a-e) to demonstrate how the relative amounts of interfacial and cohesive failure (expressed as a percentage of the total fracture area) changes with different surface treatment. Area fraction analysis was performed on each of these surfaces to provide a quantitative analysis of the

ratio of interfacial to cohesive failure of each surface. In Table 4.6 the results of this analysis are presented along with the threshold value for each condition. As expected, analysis indicated that the degree of interfacial failure varies from 100% for the untreated surface less than 10% for the 15 minute etched-only specimens. Furthermore, the degree of interfacial failure is directly related to the ΔG_{th} value, with a maximum approached as 100% cohesive failure is approached.

Table 4.6: Relative amounts of interfacial and cohesive failure for different surface conditions

Surface condition	% Interfacial	% Cohesive	ΔG_{th} (J/m^2)
Untreated	100	0	31
15 minute etched	5	95	54
30 minute etched	55	45	41
15 HT	20	80	47
30 HT	60	40	38

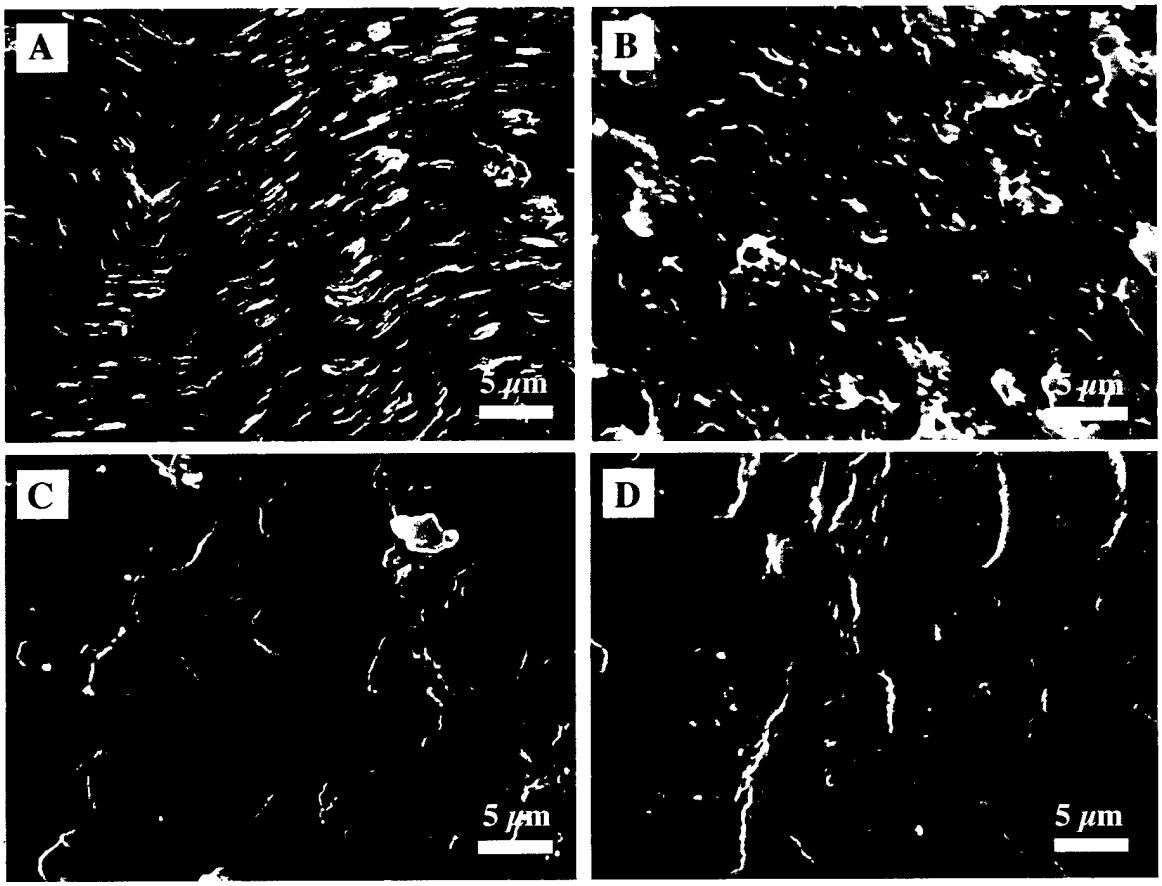

Figure 4.26: Interfacial and cohesive regions of fracture on heat treated specimens

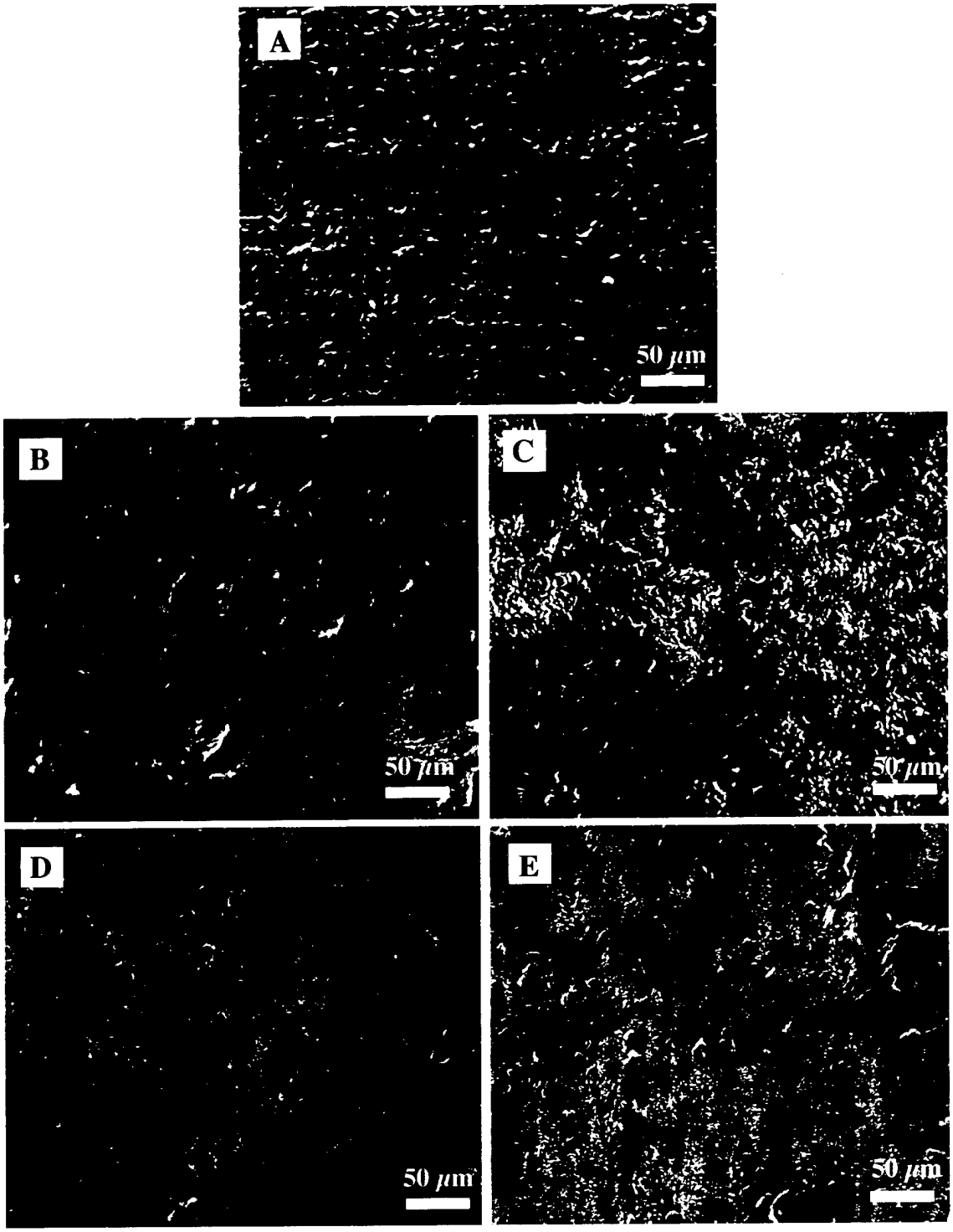

Figure 4.27: Power law regime fracture surfaces of different surface conditions: (a) untreated; (b) 15 minute etched-only; (c) 30 minute etched-only; (d) 15 HT; (e) 30 HT

Chapter 5

Discussion and Analysis

5.1 Surface Chemistry and Morphology

Researchers have been studying the chemical and morphological effects of plasma treatment on the surface of graphite fibers since the late 1980s[22-24,36-48,84]. These investigations have revealed that with the proper choice of gas and plasma operating parameters, significant changes can be made to the graphite surface. Although the exact type and extent of these changes remains a topic of considerable debate, the important role of such factors in adhesion at the graphite/epoxy interface is commonly acknowledged. Therefore, a brief discussion of the chemical and morphological changes caused by the etching process employed in this investigation is warranted.

As demonstrated in Table 4.1, the concentration of surface oxygen on the PG substrates used in this study quickly reached a saturation point after which it remained effectively constant. This saturation phenomena has also been observed by Nakahara and Sanada[6] for oxygen plasmas, as well as by Jones and co-workers[44,45] for air and argon plasmas. While some debate exists as to whether the steady-state oxygen concentration occurs at or below a maximum concentration, most researchers have reported that the phenomenon occurs rapidly. If the active sites on the graphite surface quickly saturate, the maximum attainable oxygen concentration should be constant for a specific graphite surface (e.g. HM versus AS type fibers); but this has not been the case. A more likely explanation is that chemical equilibrium is reached in the oxidation reaction[15] between the plasma and the graphite surface. In other words, the rate at which additional oxygen-containing groups are added to the surface by the plasma is equivalent to the rate of removal of these groups through further oxidation to CO_2 via the following reactions:

$$C + O \quad <--> \quad CO \qquad [5.1]$$

$$CO + O \quad <--> \quad CO_2 \qquad [5.2]$$

The saturation phenomena would thus depend on conditions such as plasma operating power and gas flow rate as well as the specific graphite surface being treated. This can therefore explain the relationship between this study and previous work on PG[6,7] in which saturation was achieved at different levels for the same surfaces when different plasma operating parameters were used.

In addition to altering surface chemistry, plasma etching can also have a dramatic effect on the morphology of graphite substrates. While most researchers agree that enhanced mechanical interlocking resulting from roughened surfaces plays a key role in adhesion, the bulk of the investigations into plasma surface treatment of carbon fibers have focused on chemical effects[18,22-24,41-43,63,89]. In these experiments, surface roughening is mentioned, but usually as an afterthought.

In this investigation, both profilometry and SEM observation revealed that plasma treatment roughened the surface to an AA roughness approximately double that of the untreated surface. Considering the fact that the surface quickly reached an oxygen saturation point, optimizing treatment time based on roughness takes on additional importance. While relatively short treatments may enable rapid processing of composites with ideal surface chemistry, such treatments minimize or even ignore the ability of etching to enhance mechanical interlocking, which may in fact be a more important factor than chemical bonding. On the other hand, care must also be taken not to over-etch the surface. As previously mentioned, over-etching causes a departure from the optimum surface roughness. Although over-etching had no effect on the overall properties of the graphite used in this study, the effects can be severe for carbon fibers where decreasing fiber strength can lead to drastic degradation in overall composite performance.

While enhancing overall surface roughness, the plasma also tended to preferentially attack irregularities in the surface which had been produced by the specimen polishing process. Others[2,34,40] have suggested that gas phase oxidation could result in such preferential attacks, but no conclusive evidence of such a process has been presented. The observation of such targeted etching indicates an opportunity for "defect engineering" of ideal morphologies. In other words, it may be possible to introduce specific defects or impurities to the surface of graphite fibers which, when subjected to an aggressive plasma, will produce specific morphologies designed to enhance mechanical interlocking at the graphite/epoxy interface.

5.2 Effect of Surface Treatment on Fatigue Crack Growth Resistance

Much effort has been made in recent decades to try to understand the quality and characteristics of the fiber/matrix interface. In the past, the interfacial shear strength (IFSS) has been widely used as a quantitative measure of the stress transfer capability between fiber and matrix. Four micromechanical testing procedures aimed at determining this parameter have often been used: fragmentation[48,55,70]; pull-out[71,72]; microbond[73]; and microcompression tests[74]. Experimental evidence from these tests supports the theory that modifications to the graphite surface, both chemical and physical, can be quite effective in improving the interfacial strength of these materials. A number of relationships between specific modifications of the graphite surface and improved interfacial properties have been proposed. Among the modifications which have been proposed to account for improved adhesion are (a) larger numbers of functional groups on the treated surfaces[75], (b) improved mechanical interlocking due to surface roughening[72], and the removal of a weak, defect-laden boundary layer from the surface[48]. Unfortunately, however, the study of interfacial adhesion between graphite surfaces and epoxy resins has been

predominantly confined to the case where static loading is considered, i.e. the relationship of interfacial adhesion to some measure of fracture toughness.

Often a more serious problem associated with fiber-based composites is the possibility that non-fatal cracks will occur along the interface between fiber and matrix. These commonly occur as the result of low-velocity impact or from manufacturing flaws such as voids in the matrix material. Under continued use of the flawed component, such cracks or defects may quickly grow to catastrophic length, depending on the ability of the material to resist crack growth. Hence, the ability to characterize the interfacial strength under conditions of repeated loading takes on added importance.

A number of attempts have been made to study fatigue crack growth in graphite/epoxy composites using entire composite laminates or coupon specimens. Several review papers[76-81] have been published which deal with the behavior of fiber-reinforced composites subjected to cyclic loading. However, serious problems arise when using full laminates in testing procedures. Although such tests provide valuable information about the overall properties of these material systems, the results are heavily dependent on such variables as fiber volume fraction, sample geometry, and fiber aspect ratio. Direct information about the fiber/matrix interface cannot be obtained by these tests.

As a result of these complications, very few investigations have been attempted which expressly deal with the influence of the fiber/matrix interface on resistance to cyclic loading. To the author's knowledge, only two studies have been published on the relationship between interfacial properties and fatigue crack growth in fibrous composites. In the first of these projects, Shih and co-workers[82] used the interlaminar shear stress (ILSS) as an indication of the interfacial strength and found that composites receiving surface treatments designed to increase ILSS also exhibited improved fatigue performance. Large-Toumi et al.[83] studied a variety of interfacial conditions to try to determine the

relationship between surface treatments and the resistance to cyclic loading. They found no clear correlation between surface treatments which increased ILSS and the resulting resistance of the composites to cyclic loading. It was found, however, that on average, those surface treatments which added oxygen to the graphite surface also lead to improved resistance to fatigue crack growth. Hence, the available literature on the subject of fiber/matrix adhesion under cyclic loading is limited, and those studies which exist do not provide specific relationships between the results of surface treatment and fatigue resistance of the fiber/matrix interface.

In the current study, an attempt was made to study the effect of modifications to a graphite surface on crack growth along the graphite/epoxy interface using the FP technique. The fatigue crack growth resistance, ΔG_{th}, followed the same trend as surface roughness. As shown in Figure 5.1, it increased initially with treatment (i.e. etching time) but then decreased as etching time was prolonged and roughness decreased.

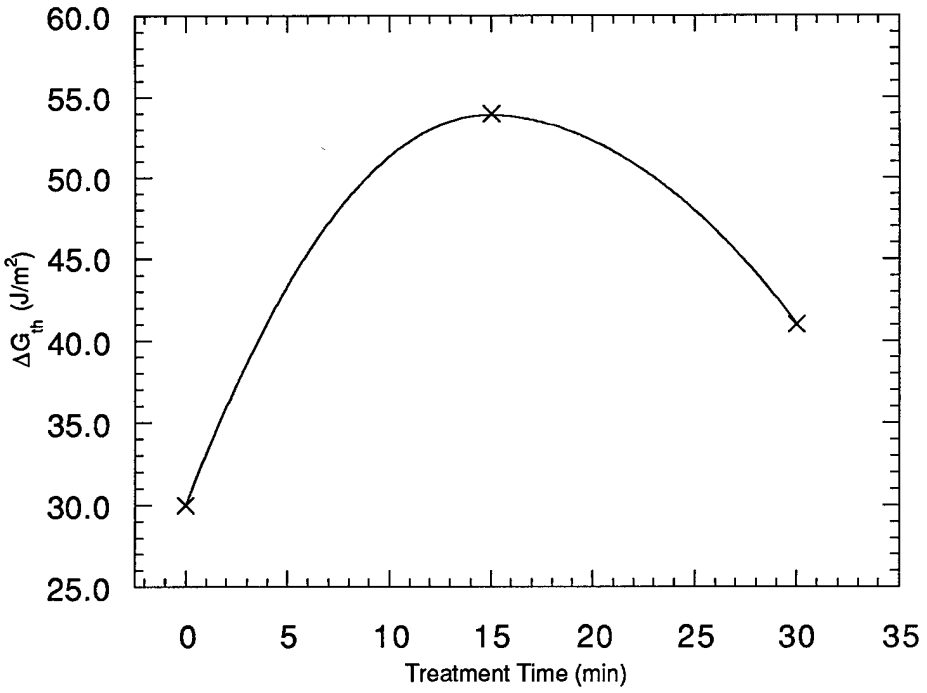

Figure 5.1: Variation of ΔG_{th} with etching time

As previously mentioned, the effects of plasma etching are not limited to surface morphology. There is an additional consideration when examining the effect of surface treatment, namely the chemical effect. Removal of the oxygen-containing functional groups added to the graphite surface during plasma etching resulted in a decrease in fatigue crack growth resistance. Recall from Figure 4.3 that the O/C ratio on the graphite surface quickly reached a saturation point, after which additional treatment did not increase oxygen content. Thus, both the 15 and 30 minute etched-only surfaces were equivalent in terms of O/C ratio and surface functionality. It was expected that restoring their O/C ratios to the untreated level would have an equal effect on the crack growth resistance of the resulting interfaces. In actuality, the value of ΔG_{th} for the 15 minute surface experienced a 13% reduction in **total** ΔG_{th} from 54J/m^2 to 47J/m^2, while the 30 minute surface experienced an 7% reduction in **total** ΔG_{th} from 41J/m^2 to 38J/m^2. However, when this reduction in interfacial strength is considered in relation to the untreated surface, the chemical effect on both treated surfaces represents slightly less than 30% of the **improved** fatigue resistance. Also, even when the scatter in experimental data is considered, as in Figure 5.2, the influence of surface chemistry, although secondary, remains a real effect.

In the only other works which similarly attempted to isolate the chemical effect on adhesion at the graphite/epoxy interface, both Drzal and co-workers[48] and Yip and Lin[24] reported that chemical bonding contributed less than 15% to improved interfacial adhesion. That chemical bonding was seen to be a smaller effect in these studies is not surprising, however. The fibers used in these studies were made of twisted graphitic ribbons, which contain a higher concentration of basal surfaces than the PG used in the current study. Since basal surfaces are known to oxidize less fully than edge sites[6], it is likely that fewer chemical bonds were formed with the adhesive. Furthermore, in the study by Yip and Lin, adhesion tests were conducted on composite laminates, the results of

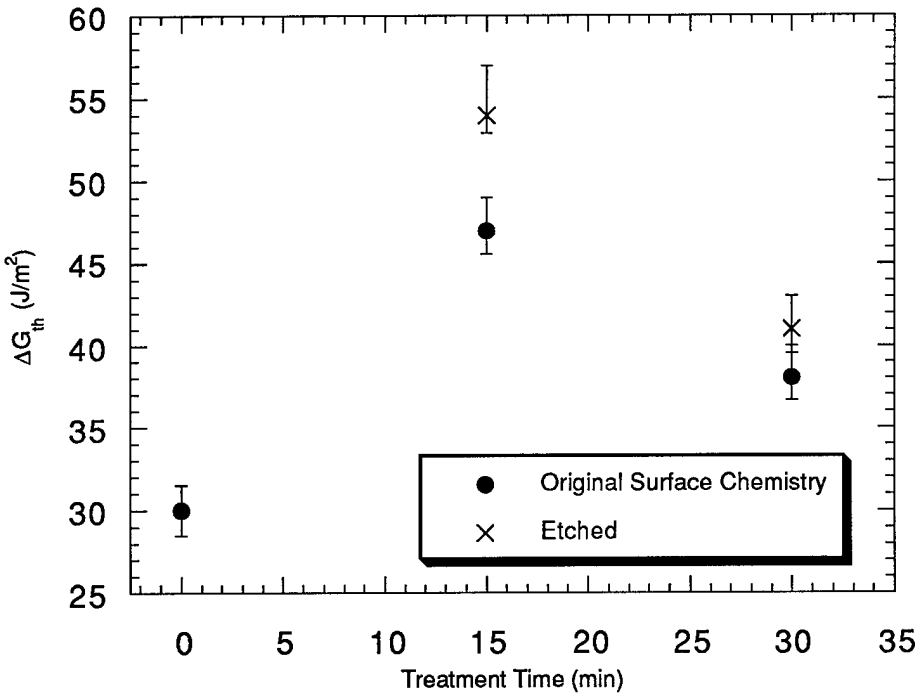

Figure 5.2: Chemical effect of etching on fatigue crack growth resistance

which were difficult to interpret due to complicating factors such as fiber-fiber interactions.

Based on the previous analysis, the following scenario is proposed to account for the surface treatment effect. The effect of plasma treatment on fatigue crack growth behavior can be characterized by two factors. The first factor, owing to surface morphology, tends to dominate the overall improvements to fatigue resistance. Essentially, by creating a more rigorous path for the crack to follow, etching provides the physical impediments to crack growth. The second factor, arising from additional chemical reactivity between adhesive and substrate, is always secondary, contributing less than 30% to the improved fatigue resistance. From Figure 5.2 it is evident that the chemical effect is coupled with the morphological effect. By optimizing surface oxygen content, plasma treatment increases crack growth resistance through stronger interfacial bonds. Together with the additional surface roughness caused by etching, the opportunity for chemical

bonding increases. Thus, the chemical strength is multiplied by the morphological contribution resulting in a greater threshold strength than would be possible for a surface modified by either parameter individually.

5.3 Failure Mechanisms

As demonstrated in sections 4.1.3 and 4.2.3, failure mechanisms varied for the different surface conditions under study. Associated with the variation in ΔG_{th} between the untreated and near-optimally treated (15 min etched) surfaces, the failure mode changed from one of completely interfacial to predominantly cohesive. The observation of a mixed failure mode (interfacial/cohesive) is not unique to this series of experiments. Instances of partial or total fracture of the adhesive in graphite/epoxy systems have been documented[40,49,90]. In fact, it has been suggested that the intrinsic upper limit of the strength at this interface depends on properties of the specific adhesive used[91].

When interfacial failure is achieved, the measured crack growth data gives an accurate assessment of the strength of the graphite/polymer interface. Change of the failure mode to cohesive failure means that the fatigue crack growth resistance of the interface is higher than what was measured and that in the strictest sense, the crack growth resistance of the interface cannot be measured. However, because the crack growth was so near the interface and the fracture energy is dissipated by plastic deformation, the resistance to near-interface crack growth becomes similar to that of an interface crack. Therefore, the measured fatigue crack growth resistance is a good representation of the interface property[92].

Furthermore, with the exception of the 15 minute etched specimens, the strength of which were almost identical to that of the adhesive (ΔG_{th} = 55J/m^2[62]), the observed thresholds are well below that of the epoxy, indicating that these values provide a

reasonable measure of the average interfacial strength for these surfaces, rather than the adhesive property. The consistency between crack growth data, surface morphology, and surface chemistry also suggests that the trend seen in the data are an accurate reflection of the effects of surface treatment on fatigue crack growth.

5.4 Modeling

The first step in designing a model for the effect of surface treatment on the fatigue crack growth resistance of the graphite/epoxy interface is to idealize the morphology of the graphite surface itself. Both before and after etching, the surface can be modeled as a series of peaks and valleys, as shown in Figure 5.3 below. In this representation, L denotes the average peak-to-peak distance, w is the width of the specimen, r is the average depth of etching, and θ is a measure of the peak-to-valley slope determined from SEM analysis of the surfaces tilted 90° to the direction of crack growth.

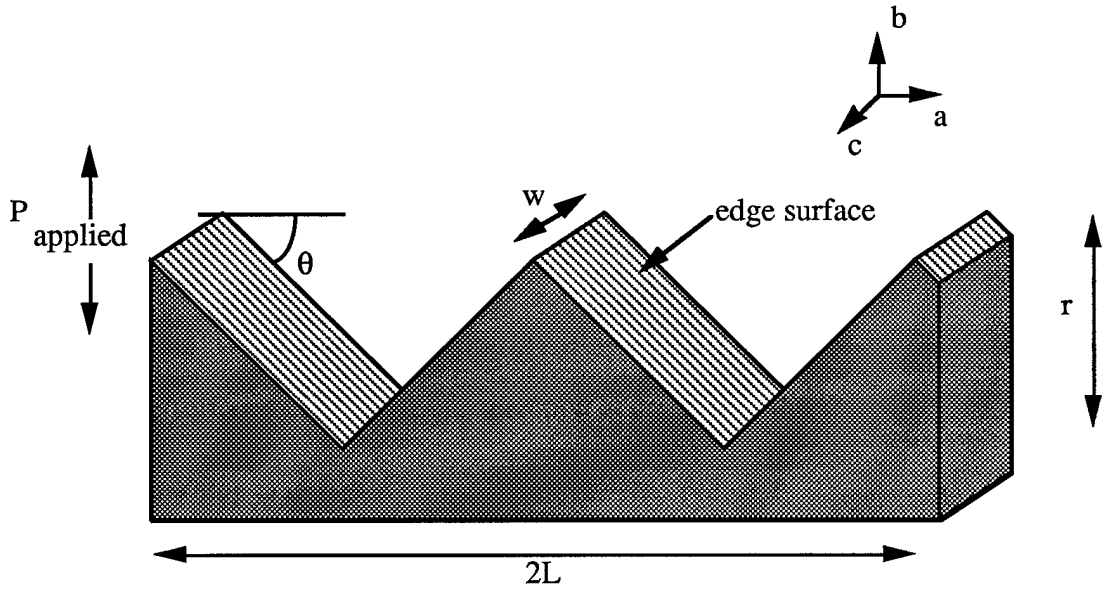

Figure 5.3: Idealized surface morphology of graphite substrates

The second step in the modeling process, is to determine the number of possible sites on the surface which can be used for chemical bonding with the epoxy adhesive. Assuming that each carbon atom on the surface has the possibility to form a chemical bond with epoxy, the number of "active sites" may be calculated from the distance between adjacent carbon atoms on hexagonal rings of each basal plane, *s*, and the distance between parallel basal planes, *l*. The product of these two distances yields the surface area which may be attributed to each bonding site, as shown in Figure 5.4.

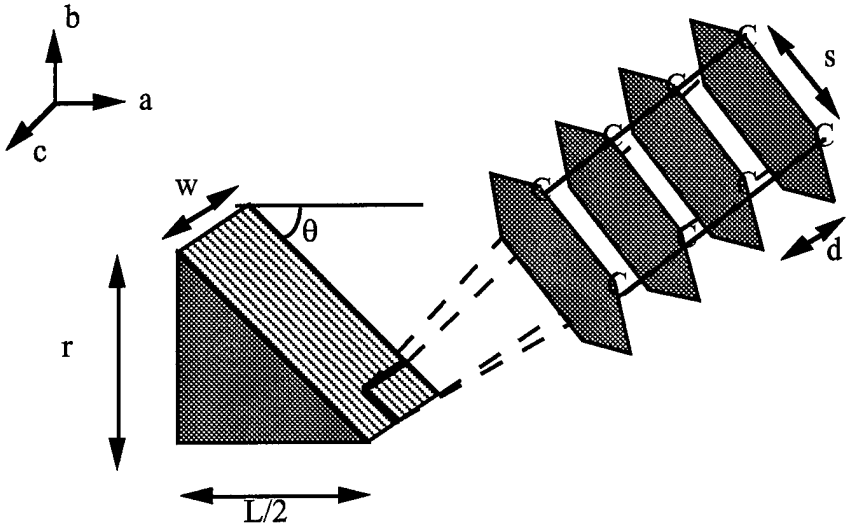

Figure 5.4: Surface area coverage per bonding site

The number of sites along the surface per peak-to-valley distance, L/2, can then be calculated as:

$$N = \frac{surface\ area}{area\ per\ site} = \frac{w \cdot \frac{L}{2} \cdot \frac{1}{\cos(\theta)}}{s \cdot d} \qquad [5.3]$$

The third step is to consider the possible types of bonding which can exist at this interface. Ehrburger and co-workers[85] and Weiss[86] have proposed a number of mechanisms through which covalent bonds can form between a functionalized graphite surface and an epoxy adhesive. Figure 5.5 presents the reactions which form these bonds. Assuming that one covalent bond of the type shown in Figure 5.5 forms at each

functionalized surface site, the average strength at one of these sites is modeled as the average of the strength of each type of bond. In a similar manner, the average strength of a non-functionalized site can be determined by assuming that only weaker electrostatic and van der Waals forces can occur. The strength at any given point on the graphite substrate can then be calculated by the following:

$$S_s = \left(mS_o + (1-m)S_u\right) \qquad [5.4]$$

where:

$S_{s:}$: average interfacial strength at any surface site (J/bond)

S_o: average strength at a functionalized site (J/bond) [87]

S_u: average strength at a non-functionalized site (J/bond) [87]

m: % oxygen on the surface

Fatigue threshold strength of the interface can then be calculated as follows:

$$\Delta G_{th} = \frac{N \cdot S_s}{nominal\ area} = \frac{\left[mS_o + (1-m)S_u\right]}{\cos(\theta) \cdot d \cdot s} \qquad [5.5]$$

Table 5.1 below summarizes the values used in the above equation to calculate threshold strength for each surface condition.

Table 5.1: Parameters for fatigue resistance model

	Surface Condition				
	Untreated	15 min etch	30 min etch	15 HT	30 HT
m	.1831	.2346	.2346	.1831	.1831
θ	10	45	25	45	25
	$S_u = 8.30 * 10^{-21}$ J/bond		d = 3.42 Å		
	$S_O = 8.30 * 10^{-19}$ J/bond		s = 1.42 Å		

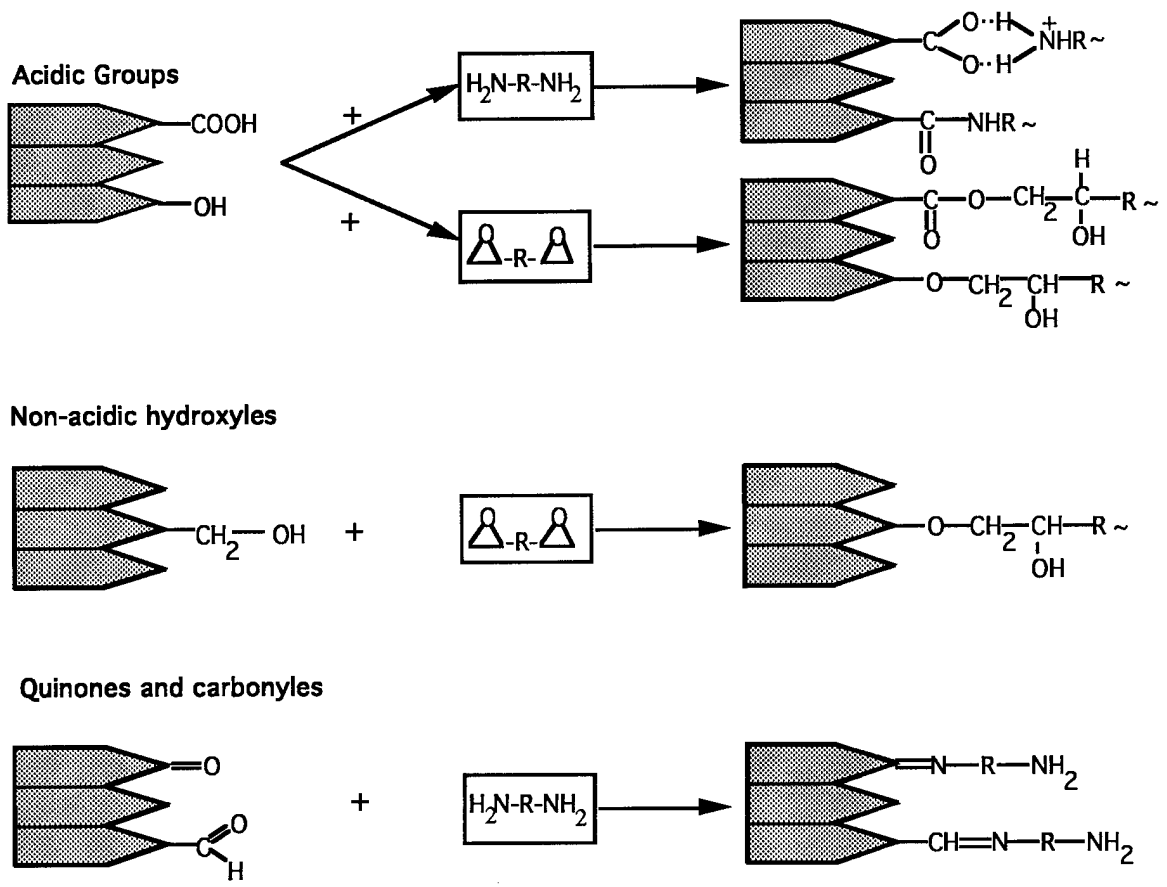

Figure 5.5: Possible reactions at carbon fiber surfaces with components of epoxy resins[85,86]

One potential shortcoming of this model is that is does not take into account the contributions of plastic dissipation energy to the overall fatigue resistance of the interface. From fracture mechanics, however, strain energy release rate can be considered to have two components:

$$\Delta G_{th} = G_o \Phi_v \qquad [5.6]$$

where Φ_v is the mechanical contribution to fatigue crack growth resistance, including plastic energy effects[88]. The plastic contributions can then be considered as a scaling constant to Equation 5.5. These effects can be removed from the model by normalizing Equation 5.5 by the ΔG_{th} of the untreated specimen. The model then predicts the trend seen in Figure 5.6.

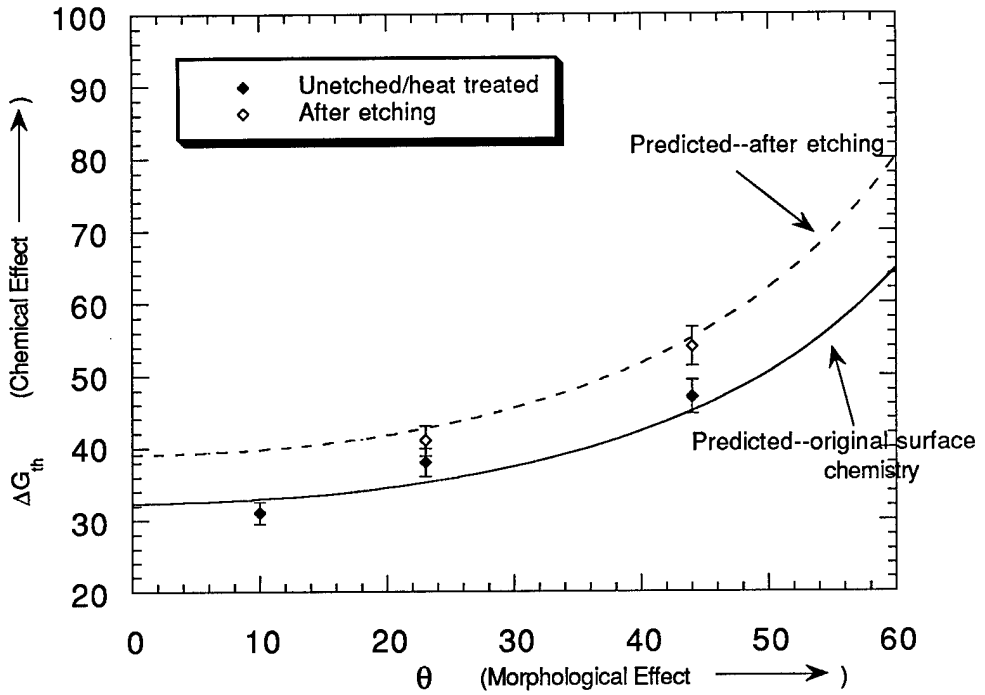

Figure 5.6: Predicted and experimental fatigue thresholds of graphite/epoxy FP specimens

From Figure 5.6, it seems that both roughness and surface chemistry play a role in achieving a strong interface. Consistent with experimental data and surface characterization, the micro-mechanical model provided a coupling effect between surface morphology and functionality. Accordingly, the model predicted that crack growth resistance could be improved either by adding additional reactive functional groups to the surface or by increasing surface roughness. In particular, the model correctly predicts the changes in the magnitude of ΔG_{th} which are directly attributable to surface chemical effects on specimens with different roughness. In the case where the surface is relatively flat, the opportunity for chemical bonding is limited and the effect is small. However, as roughness increases, the magnitude of the chemical contribution improves. Nevertheless, these results help to emphasize that even at optimum conditions, surface chemistry is never more than a secondary effect in the determination of overall fatigue resistance.

Chapter 6

Conclusions

Using PG substrates, the effects of surface treatment on graphite/epoxy adhesion were examined in more detail than is possible using either single fiber tests or laminate testing. Flexural peel specimens offer an idealized representation of this composite system while avoiding such complicating factors as fiber volume fraction and laminate lay-up. Furthermore, the FP geometry allows for observation of subcritical crack growth which runs consistently along the interface. This investigation of fatigue crack growth at the graphite/epoxy interface has led to the following conclusions:

1. Treatment of graphite substrates with an oxygen plasma has two effects on the surface. First, the plasma significantly roughens the surface by attacking irregularities or defects already present. Surface roughening through etching is only possible to a certain point, however, after which further treatment results in a loss of roughness. Second, the plasma adds reactive, oxygen-containing functional groups to the surface. Concentration of these groups quickly saturates, showing no significant changes thereafter.
2. The functional groups added to the graphite surface by plasma etching can be removed by high temperature annealing followed by hydrogen reduction. This process has no significant effect on the morphology of the graphite substrates.
3. Microwave plasma etching of graphite improves adhesion at the graphite/epoxy interface primarily by roughening the surface. The roughened surface provides a more rigorous path for an interfacial crack to follow and results in an increased amount of mechanical interlocking between the adhesive and the substrate.

4. Chemical bonding between graphite substrates and epoxy adhesives plays a secondary role in adhesion, accounting for less than 13% of the total resistance to fatigue crack growth.
5. In order to model the effects of chemical bonding on adhesion at the graphite/epoxy interface, a model was developed to account for the coupling between the chemical and morphological contributions to adhesion. This model correctly predicts the relative effects of chemistry and morphology for a variety of surface conditions.

References

1. Turbak, A.F. and Vigo, T.I. in "High-tech Fibrous Materials," A.F. Turbak and T.L. Vigo, eds., ACS Symposium Series, American Chemical Society, Washington, D.C., 1991, p. 1.
2. Krekel, G., Huttinger, K.J., Hoffman, W.P., and Silver, D.S. "The Relevance of the Surface Structure and Surface Chemistry of Carbon Fibers in Their Adhesion to High-Temperature Thermoplastics: Part I. Surface Structure and Morphology," Journal of Materials Science, **29**, 1994, pp. 2968-2980.
3. Nakahara, M., Nakoyama, Y., Katagari, G., and Shimizu, K. "Anodic Oxidation Effects on Pyrolitic Graphite Surfaces in Acid," Journal of Materials Science, **26**, 1991, pp. 861-864.
4. Nakahara, M. and Shimizu, K. "Effects of Electrolyte on the Structure of Pyrolitic Graphite Surfaces in Anodic Oxidation," Journal of Materials Science, **27**, 1992, pp. 1207-1211.
5. Shimizu, K., Nakahara, M., and Noguchi, K. "Interfacial Debonding Strength Between the Edge Surfaces of Pyrolitic Graphite and Epoxy Resins," Journal of Materials Science, **27**, 1992, pp. 6134-6140.
6. Nakahara, M. and Sanada, Y. "Modification of Pyrolitic Graphite Surface with Plasma Irradiation," Journal of Materials Science, **28**, 1993, pp. 1327-1333.
7. Nakahara, M. and Sanada, Y. "Structural Changes of a Pyrolitic Graphite Surface Oxidized by Electrochemical and Plasma Treatment," Journal of Materials Science, **29**, 1994, pp. 3193-3199.

8. Nakahara, M. and Sanada, Y. "FT-IR ATR Spectroscopy of the Edge Surface of Pyrolitic Graphite and Its Surface/PVC Interface," Journal of Materials Science, **30**, 1995, pp. 4363-4368.

9. Nakahara, M., Asai, S., Sanada, Y., and Ueda, T. "Modification of Oxidized Graphite Edge Surface with Poly(vinyl chloride)," Journal of Materials Science, **30**, 1995, pp. 5667-5671.

10. Kaeble, D.H., Dynes, R.J., Crone, L.W., and Maus, L. "Interfacial Mechanisms of Moisture Degradation in Graphite-Epoxy Composites," Journal of Adhesion, 7, 1976, p. 25-54.

11. Dauksys, R.J. "Graphite Fiber Treatments Which Affect Surface Morphology and Epoxy Bonding Characteristics," Journal of Adhesion, **5**, 1973, p. 211-244.

12. McKee, D.W. and Mimeault, V.J. "Surface Properties of Carbon Fibers," in Chemistry and Physics of Carbon, Vol. 8, P.L. Walker, Jr. and P.A. Thrower, eds., Marcel Dekker, 1973, pp. 151-241.

13. Ehrburger, P. and Donnet, J.B. "Carbon and Graphite Fibers," in High Technology Fibers, Part A, M. Lewin and J. Preston, eds., Marcel Dekker, New York, 1985, pp. 169-219.

14. Ehrburger, P. and Donnet, J.B. "Surface Treatments of Carbon Fibers for Resin Matrices," in Strong Fibers, W. Watt and B.V. Perov, eds., North-Holland, Amsterdam, 1985, pp. 577-603.

15. Vaidyanathan, N.P., Kabadi, V.N., Vaidyanathan, R., and Sadler, R.L. "Surface Treatment of Carbon Fibers Using Low Temperature Plasma," Journal of Adhesion, **48**, 1995, pp. 1-24.

16. Herrick, J.W. 23rd Ann. Tech. Conf. SPI Reinforced Plastics/Composites Division, Section 16-A, Feb. 1968.

17. Herrick, J.W., Gruber, P.E. Jr., and Mansun, F. "Surface Treatments for Fibrous Carbon Reinforcements," in AFML-TR-66-178. Part I, Air Force Materials Laboratory, July 1966.

18. Fitzer, E., Giegel, K.H., Huttner, W., and Weiss, R. "Chemical Interactions Between the Carbon Fiber Surface and Epoxy Resins," Carbon, **18**, 1979, pp. 389-393.

19. Cziollek, J., Fitzer, E., and Weiss, R. Carbon '80: 3rd International Carbon Conference, Baden-Baden Preprints, 1980, p. 632.

20. Hammin, Z. and Lin, C. "Investigation on Interfacial Effect of Carbon Fiber/Polyurethane Composites," in Interfaces in Polymer, Ceramic, and Metal Matrix Composites, H. Ishida, ed., Elsevier Science Publishing, New York, 1988, pp. 335-343.

21. Bahl, O.P., Mathur, R.B., and Dhami, T.L. "Effects of Surface Treatment on the Mechanical Properties of Carbon Fibers," Polymer Engineering Science, **24**, No. 7, 1984, pp. 455-459.

22. Bansal, R.C. and Chhabra, P. "Studies in Surface Properties of Carbon Fibers: 2. Effect of Surface Oxidation of Surface Areas of Polyacrylonitrile," Indian Journal of Chemistry, **20A**, 1981, p. 449.

23. Bansal, R.C., Chhabra, P., and Puri, B.R. "Surface Properties of Carbon Fibers: 1. Surface Oxidation of Polyacrylonitrile Based Carbon Fibers and Formation of Surface Oxygen Complexes," Indian Journal of Chemistry, **19A**, 1980, p. 1149.

24. Yip, P.W. and Lin, S.S. "Effect of Surface Oxygen on Adhesion of Carbon Fiber Reinforced Composites," Material Research Society Symposium Proceedings Vol. 170, 1990, pp. 339-344.

25. Proctor, A. and Sherwood, P.M.A. "X-ray Photoelectron Spectroscopic Studies of Carbon Fiber Surfaces. II. The Effect of Electrochemical Treatment," Carbon, **21**, 1983, pp. 53-59.

26. Koslowski, C. and Sherwood, P.M.A. "X-ray Photoelectron Spectroscopic Studies of Carbon Fiber Surfaces. IV. The Effect of Electrochemical Treatment in Nitric Acid," J. Chem. Soc. Faraday I, **80**, 1984, pp. 2099-2107.

27. Koslowski, C. and Sherwood P.M.A. "X-ray Photoelectron Spectroscopic Studies of Carbon Fiber Surfaces. V. The Effect of pH on Surface Oxidation," J. Chem. Soc. Faraday I, **21**, 1985, pp. 2745-2756.

28. Koslowski, C. and Sherwood, P.M.A. "X-ray Photoelectron Spectroscopic Studies of Carbon Fiber Surfaces. VII. Electrochemical Treatment in an Ammonium Salt Electrolyte," Carbon, **24**, 1986, pp. 357-363.

29. Koslowski, C. and Sherwood, P.M.A. "X-ray Photoelectron Spectroscopic Studies of Carbon Fiber Surfaces. VIII. A Comparison of Type I and Type II Carbon Fibers and Their Interaction With Thin Resin Films," Carbon, **25**, 1987, pp. 751-760.

30. Verbist, J.J. and Lefebvre, C. "Surface Modification of Carbon Fibers for Advanced Composite Materials," Interfacial Phenomena in Composite Materials '89, F.R. Jones, ed., Butterworths, University of Sheffield, Sheffield, U.K., 5-7 Sept. 1989, pp. 85-87.

31. Wang, T.J. and Sherwood, P.M.A. "X-ray Photoelectron Spectroscopic Studies of Carbon Fiber Surfaces. XVII. Interfacial Interactions Between Phenolic Resin and Carbon Fibers Electrochemically Oxidized in Ammonium Carbonate Solution and Their Effect on Oxidation Behavior," Chemistry of Materials, **7**, 1995, pp. 1020-1030.

32. Wang, T.J. and Sherwood, P.M.A. "X-ray Photoelectron Spectroscopic Studies of Carbon Fiber Surfaces. XVII. Interfacial Interactions Between Phenolic Resin and Carbon Fibers Electrochemically Oxidized in Nitric Acid and Phosphoric Acid Solutions and Their Effect on Oxidation Behavior," Chemistry of Materials, **6**, 1994, pp. 788-795.

33. Baillie, C.A. and Bader, M.G. "Some Aspects of Interface Adhesion of Electrolytically Oxidized Carbon Fibers in an Epoxy Resin," Journal of Materials Science, **29**, 1994, pp. 3822-3836.

34. Molleyre, F. and Bastick, M. "Carbon Fiber Treatment by Gas-Phase Oxidation," Proceedings of the 4th London International Conference on Carbon and Graphite, Soc. Chem. Ind., London, 1974, p. 190.

35. Clark, D., Wadsworth, N.J., and Watt, W. "The Surface Treatment of Carbon Fibers for Increasing the Interlaminar Shear Strength of CFRP," Proceedings of the 2nd Carbon Fibre Conference, The Plastics Institute, London, 1974, pp. 44-51.

36. Goan, J.C., US Patent 3 634 220 (1972).

37. Hou, K.C., US Patent 3 745 104 (1973).

38. Goan, J.C., US Patent 3 776 829 (1973).

39. Fujimaki, H. et al., US Patent 4 009 305 (1977).

40. Mujin, S., Baorong, H., Yisheng, W., Ying, T., Weiqiu, H., and Youxian, D. "The Surface of Carbon Fibers Continuously Treated by Cold Plasma," Composites Science and Technology, **34**, 1989, pp. 353-364.

41. Allred, R.E. and Schimpf, W.C. "CO_2 Plasma Modification of High-Modulus Carbon Fibers and Their Adhesion to Epoxy Resins," Journal of Adhesion Science and Technology, **8**, No. 4, 1994, pp. 383-394.

42. Xie, Y. and Sherwood, P.M.A. "X-ray Photoelectron Spectroscopic Studies of Carbon Fiber Surfaces. IX. The Effect of Microwave Plasma Treatment on Carbon Fiber Surfaces," Applied Spectroscopy, **43**, 1989, pp. 1153-1158.

43. Xie, Y. and Sherwood, P.M.A. "X-ray Photoelectron Spectroscopic Studies of Carbon Fiber Surfaces. XII. The Effect of Microwave Plasma Treatment on Pitch-Based Carbon Fiber Surfaces," Applied Spectroscopy, **44**, 1990, pp. 797-803.

44. Jones, C. and Sammann, E. "The Effect of Low Power Plasmas on Carbon Fiber Surfaces," Office of Naval Research and University of Illinois at Urbana-Champaign Composites Program Technical Report No. 16, October 1989.

45. Jones, C. and Sammann, E. "The Effect of Low Power Plasmas on Carbon Fiber Surfaces," Office of Naval Research and University of Illinois at Urbana-Champaign Composites Program Technical Report No. 18, October 1989.

46. Allred, R.E. and Stoller, H.M. Proceedings of the 20th International SAMPE Conference, 1988.

47. Zang, B.Z., Das, H., Hwang, L.R., and Chang, T.C. "Plasma Treatments of Fiber Surfaces for Improved Composite Performance," in Interfaces in Composites, C.G. Patano and E.J.H. Chen, eds., Materials Research Society Proceedings, Vol. 170, Materials Research Society, Pittsburgh, P.A., 1990, pp. 339-344.

48. Drzal, L.T., Rich, M.J., and Lloyd, P.F. "Adhesion of Graphite Fibers to Epoxy Matrices: I. The Role of Fiber Surface Treatment," Journal of Adhesion, **16**, 1982, pp. 1-30.

49. Drzal, L.T. "Fiber-Matrix Interphase Structure and Its Effect on Adhesion and Composite Mechanical Properties," in Controlled Interphases in Composite Materials, H. Ishida, ed., Elsevier Science Pub., New York, 1990, pp. 309-320.

50. Shyne, J.J. and Milewski, J.V. 24th Annual Technical Conference, Reinforced Plastics/Composites Division, The Society of the Plastics Industry, Inc., 1969, Sect. 18-D, pp. 1-4.

51. McGowan, H.C. and Milewski, J.V. 24th Annual Technical Conference, Reinforced Plastics/Composites Division, The Society of the Plastics Industry, Inc., 1969, Sect. 2-A, pp. 1-8.

52. Milewski, J.V. US Patent 3 580 731 (1971).

53. Downs, W.B. and Baker, R.T.K. "Modification of the Surface Properties of Carbon Fibers Via the Catalytic Growth of Carbon Nanofibers," Journal of Materials Research, **10**, No. 3, 1995, pp. 625-633.

54. Reiss, G., Bourdeaux, M., Brie, M., and Jouquet, G. "Carbon Fibers-Their Place in Modern Technology," Proceedings of the 2nd Carbon Fibre Conference, The Plastics Institute, London, 1974, p. 52.

55. Drzal, L.T., Rich, M.J., Koening, M.F., and Lloyd, P.F. "Adhesion of Graphite Fibers to Epoxy Matrices: II. The Effect of Fiber Finish," Journal of Adhesion, **16**, 1983, pp. 133-152.

56. Okhuysen, B., Cochran, R.C., Sposili, R., and Donnellan, T.M. "Interface/Interphase Studies in Epoxy Matrix Composites," Journal of Adhesion, **45**, 1994, pp. 3-14.

57. Commercon, P. and Wightman, J.P. "Effect of Organic Gas Plasmas on the Adhesion of Matrix Resins to Carbon Fibers," Journal of Adhesion, **47**, 1994, pp. 257-268.

58. McAllister, P. and Wolf, E.E. "Ni Catalyzed Carbon Infiltration of Carbon Fiber Substrates," Carbon, **30**, 1982, pp. 189-200.

59. Zielinski, R.E. and Grow, D.T. "An Iron Catalyst for CVD of Methane on Carbon Fibers," Carbon, **30**, 1992, pp. 295-299.

60. Gebhardt, J.J. "Surface Effects in Pyrolitic Infiltration of Carbon Fiber Preforms," 14th Biennial Conference on Carbon, Pennsylvania State University, PA., Extended Abstracts, 1979, p. 232.

61. Advanced Ceramics, Technical Information Sheet, 1985.

62. Zhang, Zhehua, "Mechanisms of fatigue Crack Growth at Polymer/Metal Interfaces," Ph.D. Thesis, University of Illinois at Urbana-Champaign, 1996.

63. Hammer, G.E. and Drzal, L.T. "Graphite Fiber Surface Analysis by X-Ray Photoelectron Spectroscopy and Polar/Dispersive Free Energy Analysis," Applications of Surface Science, **4**, 1980, pp. 340-355.

64. Yao, Daping and Shang, J.K. "Effect of Aging on Fatigue Crack Growth at Sn/Pb/Cu Interfaces," Metallurgical and Materials Transactions A, **26A**, 1995, pp. 2677-2685.

65. Zhang, Zhehua and Shang, J.K. "Subcritical Crack Growth at Bimaterial Interfaces: Part I: Flexural Peel Technique," Metallurgical and Material Transactions A, **27A**, 1996, pp. 205-211.

66. Lukyanov, I.M., Shchukarev, A.V., Smirnov, E.P., and Aleskovski, V.B., Theoretical and Experimental Chemistry, **58**, 1986, p. 455.

67. Fitzer, E. and Weiss, R. "Effect of Surface treatment and sizing of C-Fibres on the Mechanical Properties of CFR Thermosetting and Thermoplastic Polymers," Carbon, **25**, 1987, pp. 455-467.

68. Riggs, D.M., Shuford, R.J., and Lewis, R.W. Ch. 11: "Graphite Fibers and Composites," in Handbook of Composites, G. Lubin, ed., Van Nostrand Reinhold, New York, 1982, pp. 196-272.

69. Chai, H. "Shear Fracture," International Journal of Fracture, **37**, 1988, pp. 137-159.

70. Basom, W.D. and Jensen, R.M. "Stress Transfer in Single Fiber/Resin Tensile Tests," Journal of Adhesion, **19**, 1986, pp. 219-239.

71. Penn, L., Bystry, F., Karp, W., and Lee, S. "Aramid/Epoxy vs. Graphite/Epoxy: Origin of the Difference in Strength at the Interface," in Molecular Characterization of Composite Interfaces, H. Ishida and G. Kumar eds., Plenum Press, New York, 1985, pp. 93-109.

72. Schadler, L.S., Laird, C., and Figueroa, J.C. "Interphase Behavior in Graphite-Thermoplastic Monofilament Composites," Journal of Materials Science, **27**, 1992, pp. 4024-4033.

73. Miller, B., Muri, P., and Rebenfeld, L. "A Microbond Method for Determination of the Shear Strength of a Fiber/Resin Interface," Composites Science and Technology, **28**, 1987, pp. 17-32.

74. Mandell, J.T., Grande, D.H., Tsaing, T.H, and McGarry, F.J., "Modified Microdebonding Test for Direct *In Situ* Fiber/Matrix Bond Strength Determination in Fiber Composites," Composite Materials: Testing and Design, ASTM STP 893, J.M Whitney, ed., American Society for Testing and Materials, Philadelphia, PA, 1986, pp. 87-108.

75. Tuinstra, F. and Koenig, J.L. "Characterization of Graphite Fiber Surfaces with Raman Spectroscopy," Journal of Composite Materials, **4**, 1970, pp. 492-499.

76. Harris, B. "Fatigue and Accumulation of Damage in Reinforced Plastics," Composites, **8**, 1977, pp. 214-220.

77. Talreja, R. "Fatigue Behavior of Composite Materials: Damage Mechanisms and Fatigue Life Diagrams," Proceedings of the Royal Society of London, **A 378**, 1981, pp. 461-475.

78. Konur, O., and Matthews, F.L. "Effect of the Properties of the Constituents on the Fatigue Performances of Composites: A Review," Composites, **20**, 1989, pp. 317-328.

79. Curtis, P.T. " The Fatigue Behavior of Fibrous Composite Materials," Journal of Strain Analysis, **24**, No. 4, 1989, pp. 235-244.

80. Hahn, H.T. "Fatigue of Composites," in Delaware Composites Design Encyclopedia, Vol. 1 - Mechanical Behavior and Properties of Composite Materials, Section 1.4, Technomic Publishing Co., 1989.

81. Reifsnider, K.L. "Damage and Damage Mechanics," in Fatigue of Composite Materials, Chapter 2, K.L. Reifsnider, ed., Elsevier Science Publishers, 1990, pp. 11-77.

82. Shih, G.C. and Ebert, L.J. "The Effect of the Fiber/Matrix Interface on the Flexural Fatigue Performance of Unidirectional Fiberglass Composites," Composites Science and Technology, **28**, 1987, pp. 137-161.

83. Large-Toumi, B., Salvia, M., and Vincent, L. "Fiber/Matrix Interface Effect on Monotonic and Fatigue Behavior of Unidirectional Carbon/Epoxy Composites," Fiber, Matrix, and Interface Properties, ASTM STP 1290, C.J. Spragg and L.T. Drzal, eds., American Society for Testing and Materials, 1996, pp. 182-200.

84. Donnet, J.B., Dhaml, T.L, Dong, S., and Brendle, J. "Microwave Plasma Treatment Effect on the Surface Energy of Carbon Fibers," Journal of Physics D: Applied Physics, **20**, 1987, pp. 269-275.

85. Ehrburger, P., Herque, J.J., and Donnet, J.B. London, Soc. Chem, Ind., **1**, 1978, p. 398.

86. Weiss, R. Ph.D. Dissertation, University of Karlsruhe, 1984.

87. Zumdahl, Steven S. Chemistry, Chapter 8: Bonding—General Concepts, D.C. Heath and Company: Lexington, Mass., 1986, p. 316.

88. Kinloch, A.J. Adhesion and Adhesives, Chapter 3: Mechanisms of Adhesion, Chapman and Hall: New York, 1987, p. 85.

89. Wu, G.M. and Schultz, J.M. "Effects of Treatment on the Surface Composition and Energy of Carbon Fibers," Polymer Composites, **16**, No. 4, 1995, pp. 284-287.

90. Hoecker, F. and Karger-Kolsis, J. "Effect of the Interface on the Mechanical Response of CF/EP Microcomposites and Macrocomposites," Composites, **25**, No. 7, 1994, pp. 729-735.

91. Drzal, L.T. "Intrinsic Limitations in Using Interphase Modification to Alter Fiber-Matrix Adhesion in Composite Materials," in Materials Research Society Symposium Proceedings, Vol. 170, 1990, pp. 275-283.

92. Zhang, Z. and Shang, J.K. "Subcritical Crack Growth at Bimaterial Interfaces: Part III. Shear-Enhanced Fatigue Crack Growth Resistance at Polymer/Metal Interface," Metallurgical and Material Transactions A, **27A**, 1996, pp. 221-227.

REPORT DOCUMENTATION PAGE	Form Approved OMB No. 0704-0188

1. AGENCY USE ONLY *(Leave blank)*	2. REPORT DATE	3. REPORT TYPE AND DATES COVERED
	12 MAY 97	

4. TITLE AND SUBTITLE
CHARACTERIZATION OF THE GRAPHITE/EPOXY INTERFACE WITH VARIOUS SURFACE TREATMENTS UNDER CYCLIC LOADING

5. FUNDING NUMBERS

6. AUTHOR(S)
JAMES PAUL RYAN

7. PERFORMING ORGANIZATION NAME(S) AND ADDRESS(ES)
GRADUATE COLLEGE OF THE UNIVERSITY OF ILLINOIS AT URBANA-CHAMPAIGN

8. PERFORMING ORGANIZATION REPORT NUMBER
97-035

9. SPONSORING/MONITORING AGENCY NAME(S) AND ADDRESS(ES)
DEPARTMENT OF THE AIR FORCE
AFIT/CI
2950 P STREET
WRIGHT-PATTERSON AFB OH 45433-7765

10. SPONSORING/MONITORING AGENCY REPORT NUMBER

11. SUPPLEMENTARY NOTES

12a. DISTRIBUTION AVAILABILITY STATEMENT

12b. DISTRIBUTION CODE

13. ABSTRACT *(Maximum 200 words)*

14. SUBJECT TERMS

15. NUMBER OF PAGES
89

16. PRICE CODE

17. SECURITY CLASSIFICATION OF REPORT	18. SECURITY CLASSIFICATION OF THIS PAGE	19. SECURITY CLASSIFICATION OF ABSTRACT	20. LIMITATION OF ABSTRACT